Dissertations, Master's Theses and Master's Reports

2023

VIRUS INACTIVATION BY NOVEL VIRUCIDAL MATERIALS

Sneha Singh
Michigan Technological University, snehas@mtu.edu

VIRUS INACTIVATION BY NOVEL VIRUCIDAL MATERIALS

By

Sneha Singh

A THESIS

Submitted in partial fulfillment of the requirements for the degree of

MASTER OF SCIENCE

In Chemical Engineering

MICHIGAN TECHNOLOGICAL UNIVERSITY

2023

This thesis has been approved in partial fulfillment of the requirements for the Degree of MASTER OF SCIENCE in Chemical Engineering.

Department of Chemical Engineering

Thesis Advisor: *Dr. Caryn Heldt*

Committee Member: *Dr. Rebecca Ong*

Committee Member: *Dr. Bruce Lee*

Department Chair: *Dr. Pradeep K. Agrawal*

Table of Contents

List of Figures

List of Tables

Author Contribution Statement

This thesis presents the evaluation and mechanism of antiviral activity by novel virucidal materials. While the thesis document was prepared by me alone, the work outlined in the thesis document was a collaborative effort.

In section 4.1, infusion of cupric ions into the clay minerals, characterization of the clay minerals using x-ray diffraction (XRD) and inductively coupled plasma mass spectrometry (ICP-MS) of the minerals to obtain metal ion release data, were completed by Dr. Bowen Li's lab. XRD figures are not included in the thesis document. The ICP-MS data is provided in Table 4.3, 7.1 and 7.2. For the SEM imaging of the powders, the powder samples were prepared by me, however, the images were obtained by Natalie Nold, a PhD candidate in the chemical engineering department. Antiviral work with two viruses were presented. All of the experiments with porcine parvovirus were completed by Vaishali Sharma (figures 4.1A, 4.2A, 4.6A, 4.7 and 4.8A), a PhD student in the biological sciences department. Any work presented with the human coronavirus (HCoV 229E) was completed by me.

In section 4.2, functionalization of the melt-blown and spun-bound polypropylene fabrics, characterization, zeta potential measurement, filtration efficiency and pressure drop measurements were completed by our collaborators at Rensselaer Polytechnic Institute (RPI), Mirco Sorci, Edmund F. Palermo, and R. Helen Zha (figures 3.1, 3.2, and 4.10 and 7.1). For the antiviral work, the suid herpesvirus (SuHV-1) data was collected by both Vaishali Sharma and me (figure 4.11 A). The HCoV 229E data was collected by me.

In section 4.3, copolymerization of polyacrylamide with 6-hydroxydopamine and dopamine methacrylamide, coating of the melt-blown polypropylene fabric, characterization, and H_2O_2 quantitation using the FOX assay were completed by our collaborator Fatemeh Razaviamri (figure 3.4, 4.13 and 4.14), a PhD candidate in Dr. Bruce Lee's research group. All of the antiviral work with bovine viral diarrhea virus (BVDV) and HCoV 229E was completed by me.

Acknowledgements

Abstract

The development of virucidal coatings to inactivate a broad spectrum of viruses has gained popularity. Antiviral coating of personal protective equipment such as facial coverings can reduce the accumulation of viral load and mitigate transmission of airborne illnesses, which occur primarily through direct contact with respiratory aerosols or droplets carrying infectious viruses. Moreover, modification of PPE to inactivate viruses upon contact improves their reusability and reduces waste. Coating high frequency touch surfaces with similar virucidal coatings can reduce the risk of disease transmission associated with contaminated surfaces. This study explores the development of three novel virucidal materials to control the spread of viruses which occur either through direct or indirect exposure.

Naturally occurring zeolites and clay minerals such as vermiculite and sepiolite find use in polymer composites to enhance material properties. They are highly absorbent and due to their large cation-exchange capacity, provide a great platform to incorporate virucidal metal ions such as silver, zinc, copper and iron. Here, two novel antiviral clay mineral powders, vermiculite, and sepiolite, were decorated with a powerful antiviral agent, cupric ion (Cu^{2+}). The modified vermiculite powders showed 2.6 and 2.5 log-reduction in the titer of the non-enveloped PPV and enveloped HCoV 229E, respectively, by inactivation in 2 hours at 4 °C. Sepiolite reduced the titers of PPV and HCoV by 3.5 and 3.2 log_{10} respectively, either through inactivation or virus adsorption or both. Adsorption of virus to the surface of the powder was determined to be crucial for inactivation by Cu^{2+}.

Quaternary ammonium (QA) compounds find use commercially and domestically to inactivate a broad spectrum of disease-causing viruses. Melt-blown polypropylene (mbPP), used as the main filtration layer in the WHO approved N95 mask and spun-bound polypropylene (sbPP), utilized in surgical masks were covalently and physically functionalized with a C_{12} quaternary ammonium compound - benzophenone. QA grafting of mbPP resulted in the largest reversal of surface charge density. The same fabric was found to be most effective in lowering the titer of enveloped viruses SuHV-1 and HCoV 229E by 3.3 and 2.3 log_{10} respectively. However, functionalization of the fabric decreased the filtration efficiency to ~50% which was resolved by using the less effective sbPP as an outer layer in a prototype 3-ply N95 mask model.

Hydrogen peroxide (H_2O_2), a strong oxidizing agent, is another disinfectant commonly used in industry and households to meet daily disinfection needs. H_2O_2 releases a highly reactive hydroxyl free radical which can disrupt a broad spectrum of biomolecules such as proteins, nucleic acids and lipids to inactivate viruses. The catechol functional group in 6-hydroxydopmine (6-OHDA) generates H_2O_2 as a by-product when exposed to moisture. Here, polyacrylamide (PAAm) copolymerized with 6-OHDA was coated onto non-woven mbPP fabrics while maintaining fabric porosity at 80%. Sustained release of H_2O_2 with catechol copolymerized mbPP fabrics was demonstrated over a 24-hour period at room temperature. The fabrics were found to show 2.2 and 1.1 log-reduction in the titer of BVDV and HCoV respectively at room temperature.

1 Introduction

The twenty first century witnessed the outbreak of several familiar as well as never before encountered deadly viral infectious diseases. The Severe Acute Respiratory Syndrome (SARS) outbreak in 2003, a highly pathogenic disease, spread to over a dozen countries and infected over 8000 people worldwide with the rate of mortality estimated to be over 10% [1]. Transmission of disease occurred primarily through the respiratory droplets of an infected individual, with the rate of transmission the highest during the onset of peak symptoms. The spread of Ebola, a fatal viral hemorrhagic illness, occurred through close bodily contact with infected individuals during the acute infection stage [2]. The Zika virus infection outbreak in 2016 had severe impact on fetal development, given infections occurred during pregnancy. Arthropod vectors carried by mosquitoes were identified as the main cause of transmission [3]. Given the highly global dynamic of the current world, these viruses encountered little to no resistance to crossing borders and infecting people worldwide. Some diseases such as SARs and Ebola were highly pathogenic while others highly transmissible. The highly transmissible COVID-19, caused by SARs CoV-2 and declared a pandemic, has, as of now, infected over 600 million people worldwide [4]. In addition to the high transmissibility, an additional challenge with COVID-19 was the ability of infected individuals to transmit virus even before the onset of symptoms. Not only symptomatic but asymptomatic infected individuals could also spread the disease [5]. Each outbreak left in its wake mass socio-economic distress, political disruption, and loss of invaluable lives. Even with numerous developments in medicine and technology, with the COVID -19 pandemic, mankind found itself immensely unequipped to swiftly initiate and implement strategies to mitigate transmission of the highly infectious SARs CoV-2 virus.

Immunization is perhaps the most effective preventative approach to protect humans from disease causing viruses. However, vaccines are developed to be highly specific and are unique to the disease-causing pathogen. Moreover, in the case of unknown viruses, identification and development of appropriate vaccine candidates requires time and resources. Even if a vaccine can be developed rapidly, scale-up efforts and production to meet demand worldwide, in a timely manner, can be challenging. Additionally, in certain rare cases, vaccination does not always result in active immunization, particularly in immunosuppressed individuals [6]. Therefore, there is an urgency to explore alternate, rapidly developable routes, designed to inhibit the spread of a broad spectrum of disease-causing viruses.

The use of conventional physical and chemical disinfectants, and engineering controls (personal protective equipment and facial coverings) gained popularity following the COVID-19 pandemic. However, these methods suffered certain limitations. Physical disinfection techniques rely on external factors for inactivation such as heat, light and UV [7]. Most chemical disinfectants such sodium hypochlorite and surfactants are harsh and hazardous to the environment [8]. Physical barriers such as facial coverings, while fairly effective against transmission, are often non-reusable, can accumulate viral burden and increase the total amount of waste generated. A more recent approach to mitigate disease transmission includes the modification of surfaces with sustainable antipathogenic

coatings. Robust knowledge of how viral diseases are transmitted, the biophysical and chemical properties of viruses and the mechanism by which they can be inactivated are fundamental to developing competent virucidal materials.

This thesis explores the development of three different types of novel virucidal materials and seeks to provide insight into their use as efficacious antiviral agents as well as their mechanism of virus inactivation. The first study tests the virucidal effect of cupric-ion (Cu^{2+}) infused clay minerals, vermiculite and sepiolite, against the non-enveloped porcine parvovirus (PPV) and the enveloped human coronavirus (HCoV-229E). The virucidal competence is compared with a known antiviral agent, cuprous oxide (Cu_2O), and their respective undecorated powders. A series of blocking experiments provided insight into the mechanism by which the clay mineral powders bring about their antiviral behavior. The second study demonstrates the antiviral efficacy of non-woven filtration fabrics, melt-blown and spun-bound polypropylene, chemically or physically modified by polymerization with C_{12}-quaternized benzophenone. The efficacy and mechanism of virus inactivation was determined using two enveloped viruses, suid herpesvirus (SuHV-1) and HCoV-229E. Lastly, the third and final study, also explores the modification of a non-woven fabric, melt-blown polypropylene with a novel copolymer composed of polyacrylamide and the catechol containing 6-hydroxydopamine (AA-DA-OH-co-AAm). The design and application of the polymer was inspired by the unique redox chemistry demonstrated by marine mussels to facilitate adhesion to surfaces under water. Enveloped bovine diarrhea virus (BVDV) and HCoV 229E were used as model viruses to demonstrate the polymers required physiological pH and moisture in order to exhibit antiviral behavior. The efficacy of the designed polymer was tested against a control copolymer containing the known antiviral agent, dopamine methacrylamide (DMA-co-AAm).

Chapter 1 provided an introduction to the thesis. Chapter 2 contains a literature review to obtain a deeper understanding of the main modes of disease transmission, the biological and physical properties of viruses, routes of virus inactivation, and lastly common tools available to inactivate viruses. An understanding of these concepts is key to designing novel virucidal materials. Chapter 3 provides a detailed description of the materials and methods utilized in the development of each of the virucidal materials as well as the methods employed to maximize virus inactivation and obtain a mechanistic understanding of the inactivation process by each material. Chapter 4 contains a summary of the results along with a detailed discussion of our main findings. Chapter 5 provides a conclusion to the thesis. Literature cited in the thesis document and the supplemental information will be provided in chapter 6 and 7 respectively.

2 Literature Review

2.1 Disease transmission

Respiratory viruses like the influenza virus or the SARS-CoV-2 virus spread through the aerosols or respiratory droplets released by an infected individual during coughing and sneezing [9, 10]. A person can produce as many as thousands of droplets and aerosols as shown in figure 2.1. Based on size, virus laden aerosols with a small aerodynamic diameter remain suspended in air while others settle on lower surfaces [5]. Two main routes of virus transmission through aerosols and droplets have been reported – direct transmission (primary transmission) and indirect transmission (secondary transmission) [5, 6, 11].

Primary Transmission

A single sneeze can produce up to **10,000 droplets**

The virus can remain **suspended in the air** in very tiny droplets

Virus entry into the respiratory tract through inhalation

Secondary Transmission

Fomites can be picked up transferring virus from hand different routes of entry

Large droplets can settle on surfaces due to gravity
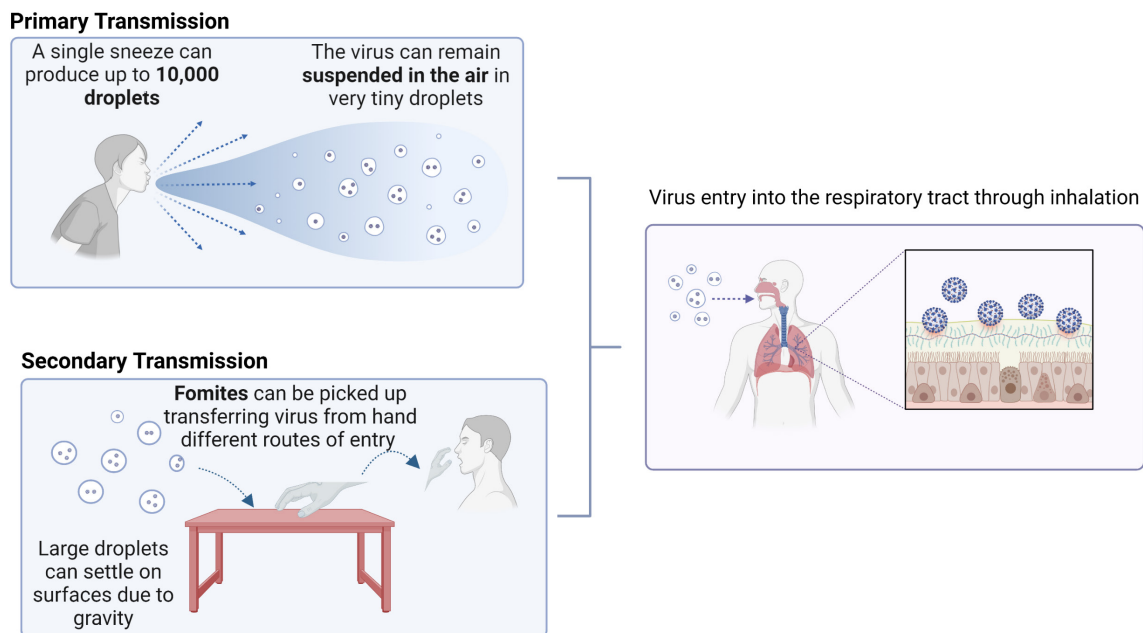
Figure 2.1: Spread of virus through primary and secondary transmission due to the aerosols and virus droplets released from the cough or sneeze of an infected individual; figure created in biorender.com, modified template "*SARS-CoV-2: How is the Virus Spread?*"

Primary or direct transmission of viruses occurs when one comes into direct contact with the pathogen. Examples of direct transmission include blood-borne transmission, fecal-oral transmission or inhalation of aerosols or droplets carrying viruses [12]. The entry of virus into the respiratory tract through the nose is perhaps the most common route for direct transmission of airborne viruses. A human can inhale up to 0.5 L of air per breath which may contain aerosols or liquid droplets with viruses [13]. Aerosols, in particular, are known to be more infectious as they can linger in air and be transmitted over short and long distances [9]. Viruses can also enter the gastrointestinal tract through the mouth, by consuming food or drinks contaminated with viral pathogens. Virus entry through the reproductive organs can also occur through sexual activity [11]. Regardless

of the route of entry, infection is generally limited to the individuals who are directly exposed.

Secondary transmission generally occurs in-directly by coming in contact with contaminated surfaces, also referred to as fomites [16]. Anyone who touches the contaminated surface and picks up the viable, infectious viral particles could potentially become infected. Contamination of high frequency touch surfaces, in particular, pose a serious threat as a single source of contamination can potentially result in multiple infections.

In either case of transmission, dose of exposure plays a vital role in the severity of disease as the virus needs to overcome the natural physical (mechanical and chemical) and internal barriers (innate and adaptive immune system) present in the human body to cause pathogenesis [11]. The brief overview of infectious diseases and how they can be transmitted shows the impact pathogenic organisms have had over human health worldwide. Bacteria, parasites, viruses and the toxins they produce are some of the most commonly known pathogenic infectious agents. The focus of this review, however, will only be on viruses. Viruses can be inactivated by modifying the virus or the host cell environment. The focus here will be on virus modification. Understanding the structure, dynamics and physicochemical properties of viruses will be crucial to developing antiviral materials.

2.2 Viruses

Viruses are small infectious units ranging in size from 10 nm to over 300 nm. Based on molecular composition, viruses can be classified as non-enveloped or enveloped (figure 2.2). A typical non-enveloped virus consists of a protein capsid and an RNA or DNA based genome [14-16]. Porcine parvovirus (PPV), norovirus, enterovirus, adenovirus and rhinovirus are some commonly known non-enveloped viruses. Enveloped viruses, on the other hand, have their capsid enclosed by a lipid envelope which contains proteins or glycoproteins acquired from the host cell. A few common examples of enveloped viruses are human coronavirus, influenza virus, HIV and RSV.
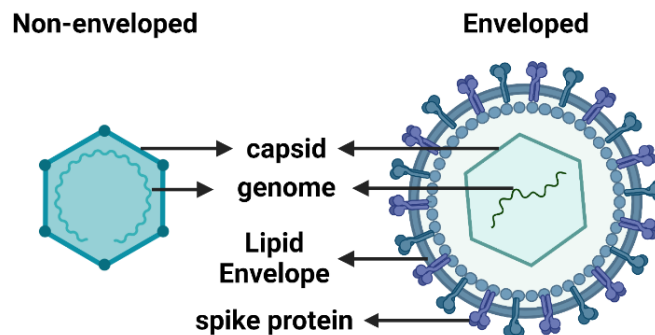
Figure 2.2: Types of viruses; enveloped Sars-CoV-2 (right) and non-enveloped porcine parvovirus (left); figure created in biorender.com

The debate on whether viruses can be considered "living" or "non-living" is still ongoing. The source of the debate arises from the inability of viruses to replicate and create more copies of themselves on their own [15]. They rely on the host cell machinery to produce more infectious particles. However, they do carry genetic information and can instruct the host cell to manufacture and assemble different viral components to give rise to fully functional, live infectious viral units [17, 18].

2.2.1 Life cycle of a virus

The life cycle of a typical virus is depicted in figure 2.3. Once a virus particle enters the body, it must be internalized by host cell. Viruses contain virus attachment proteins, highly specific to a target cell surface receptor (step 1). These proteins are located in the viral envelope in enveloped viruses. Whereas, in non-enveloped viruses, the capsid proteins facilitate surface attachment [18]. Due to the crucial role viral proteins play in cell infection, a variety of antiviral agents are developed with the aim to inhibit virus binding to the cell and prevent infection. After binding to specific membrane receptors, viruses penetrate the host cell through two modes, endocytic or non-endocytic (step 2). Endocytic virus internalization occurs through clathrin (adenovirus) or caveolae (SV40) mediated endocytosis. Clathrin mediated endocytosis is the most common means to internalize extracellular cargos in mammalian cells. It involves the assembly of cytoplasmic proteins into clathrin coated pits and remodeling of the plasma membrane to enable internalization of transmembrane receptors and ligands [19]. Caveolae are plasma membrane invaginations composed mostly of detergent resistant cholesterol and sphingolipids or "lipid rafts" and can internalize extracellular cargos [20].). Entry through this route involves pH induced conformational changes of the viral proteins or cell membrane receptors [21, 22]. Both enveloped and non-enveloped viruses take advantage of this receptor mediated endocytic pathway to gain entry into the cell [18]. Non-endocytic internalization requires crossing the host cell membrane through penetration (non-enveloped viruses) or fusion (enveloped viruses like HIV-1). Following internalization, the capsid is removed or degraded to release the virus genome (step 3). The virus genome is released and transported to the nucleus through nuclear pores. The genome carries information for the synthesis of viral proteins and genome replication, vital for the creation of new virions. Viral genetic material, once in the nucleus, is integrated into the host cell genome to make more copies of the viral genome (step 4, 5 and 6). The newly synthesized viral components are assembled to form immature viral particles (step 7). The location of assembly depends largely on the type of virus. For example, non-enveloped DNA viruses are assembled within the nucleus. Exit from the nucleus often involves cell lysis and apoptosis. Enveloped viruses, on the other hand, congregate near the plasma membrane and acquire the host cell membrane as they bud from the cell (step 8 and 9). Viruses can undergo maturation before or after release into the extracellular environment to become full functional infectious units [18].
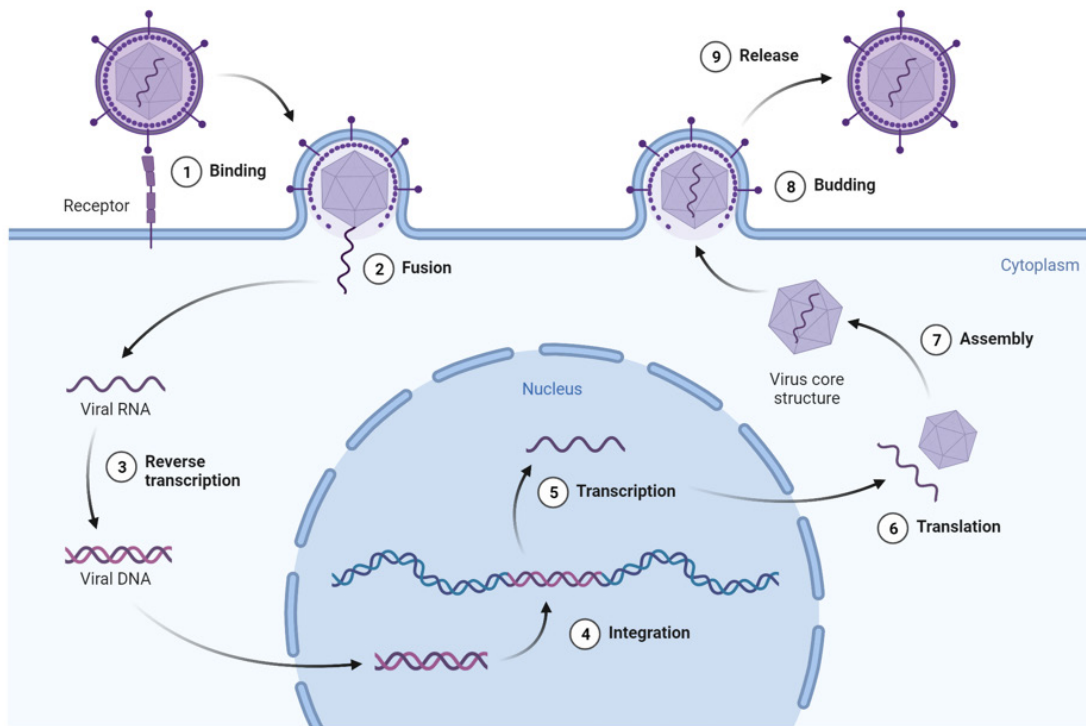
Figure 2.3: Life cycle of a typical enveloped virus; "*Generic Viral Life Cycle*" template from biorender.com

2.2.2 Virus structure

A virus consists of several components shown earlier in figure 2.2. A non-enveloped virus only has the protein capsid and the nucleic acid genome. In enveloped viruses, a protective lipid membrane surrounds the protein capsid and interacts with the capsid through matrix proteins. Irrespective of the type of virus, it may have highly specific surface proteins or spike proteins. Each viral component plays a key role in facilitating infection and can therefore be targeted to disrupt the virus life cycle.

The capsid plays a key role in virus architecture and biology. It is characterized as a protein oligomer or multimer made up of several replicas of one or a few different proteins. This oligomerization gives rise to highly symmetric structures. Visualization of these structures has become possible with the aid of several techniques such as cryo-electron microscopy, cryo-electron tomography, atomic force microscopy, and x-ray crystallography [23]. Most viruses are known to have rod-like or spherical geometry as shown in figure 2.4. Rod-like virus capsids exhibit helical symmetry where the viral capsid protein winds around a helical nucleic acid. Spherical viral capsids exhibit icosahedral symmetry. The capsid is composed of 20 faces, each one an equilateral

triangle. It exhibits 2-3-5 symmetry indicating the possible ways the icosahedron can rotate around an axis. Proteins within the capsid spontaneously interact with bonds, angled appropriately, to form the icosahedron structure [12, 14, 15]. The capsid provides structural stability and plays a critical role in protecting the virus against environmental stresses [24]. The shape of the capsid is also significant as it may provide identifying information regarding the virus and its life-cycle [16]. For example, in the case of certain helical viruses, the capsid proteins begin wrapping the genome immediately after it is copied. Whereas, in the case of icosahedral viruses, the genome may not inserted until capsid assembly is near complete [18].
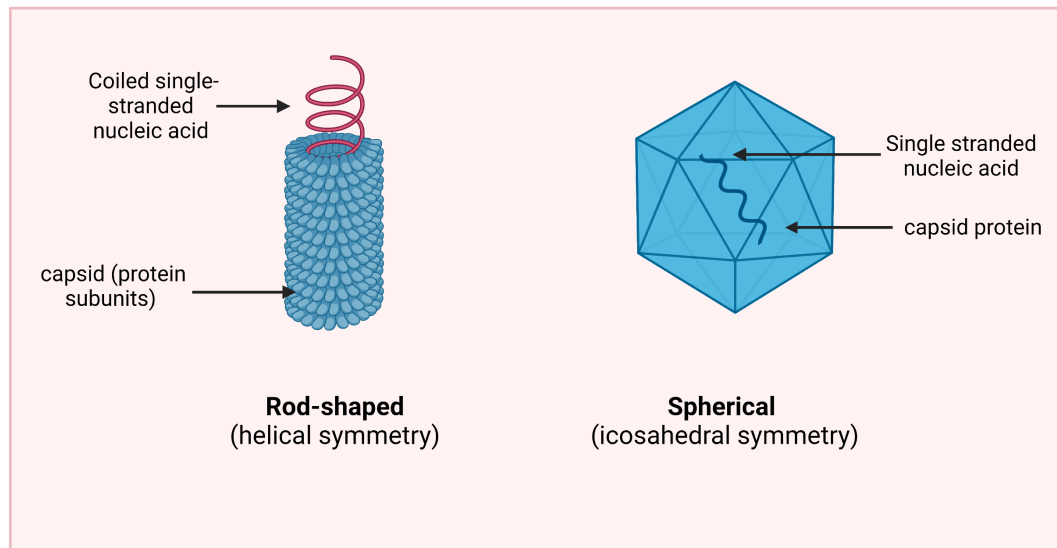
Figure 2.4: Helical (left) and icosahedral (right) symmetry observed in rod-shaped and spherical viruses respectively; figure created in biorender.com.

The genome can be composed of either DNA or RNA with each being either single stranded or double stranded. No known case of a virus genome containing both RNA or DNA has yet been reported. They can be linear, circular, segmented or non-segmented in conformation [18]. Just as there exists a large variation in the size of the virus particle, the typical size of a virus genome can vary from as little as 1-2 kilobase pairs to well over 200 kilobase pairs (kb) [14]. The increase in genome length increases the susceptibility of the molecule to breakage. ssDNA viruses are the smallest viruses with genomes as small as 1-2 kbs. They encode for 2 proteins only, one to facilitate capsid formation and another for genome replication. Conversely, dsDNA viruses, such as those belonging to the adenoviridae and herpiviridae, show higher complexity and contain 30-40 and 235 kbp respectively [25]. RNA containing viruses (riboviruses) carrying a single stranded RNA (ssRNA) or double stranded RNA (dsRNA) can be distinguished as being sense or antisense or (+)ve or (-)ve.[23].

The phospholipid bilayer is acquired by enveloped viruses as they bud and exit from the host cell. The envelope serves as a protective coat for the viral genome and

capsid. While most enveloped viruses bud from cell plasma membrane, some are known to bud from the golgi apparatus (bunyaviruses), endoplasmic reticulum (coronaviruses) and nuclear membrane (herpesviruses). The source of the viral envelope greatly influences the characteristics of the envelope [26]. They also house glycoproteins to facilitate attachment and entry of the virus into the host cell. Viral proteins play a key role in the virus life cycle. They facilitate attachment of the virus to the host cell membrane and allow the virus to be internalized by the cell. For example, the glycoprotein gp120 in the HIV-1 virus envelope has a binding site for a specific cell receptor on the surface of CD4 T cells. Several antiviral drugs have been developed to serve as "gate keepers" to prevent viral proteins from performing their role in virus replication. They either inhibit attachment of virus to the cell surface or virus fusion and penetration into the cell [27].

The virus structure and life cycle can provide useful information on virus persistence, survival and ability to cause infection. Enveloped viruses rely on the lipid membrane and surface proteins to facilitate internalization into the cell [22, 28]. However, the envelope itself is quite fragile and makes the virus more susceptible to inactivation by heat, desiccation, alcohol and detergents outside of the host [29]. On the other hand, the envelope offers certain benefits as well. It provides structural flexibility and enables the virus spike proteins to evade recognition by the host's immune system. It also protects the virus during egress from the host cell [16, 29]. Non-enveloped viruses, in general, are environmentally stable as they lack the lipid bilayer and rely on capsid proteins for cell recognition and attachment. They often tend to be found in extreme environments [16, 30] and require relatively harsher conditions for inactivation [31].

2.3 Factors affecting virus stability

The persistence of viable viruses in air and on surfaces is a major contributing factor to disease transmission. Several studies have documented the ability of viruses to persist and remain viable in air and surfaces anywhere from < 5 min to over 28 days on surfaces [32]. The type of virus along with environment factors such as temperature, pressure, relative humidity (RH), surface porosity and surface sorption affect the ability of viruses to persist and maintain viability[16].

2.3.1 Environmental factors

Increasing temperature has been linked with faster progression of virus inactivation in comparison to lower temperatures [33, 34]. A study on the effect of temperature on Norwalk virus-like particles (VLPs) showed a negative effect of temperatures over 55 °C on virus stability [33]. The VLPs were found to undergo dramatic changes in the secondary, tertiary, and quaternary structures of the capsid protein. Changes in the tertiary structure were attributed to the aromatic residues Phe, Tyr and Trp found in the VP1 protein. Changes in the microenvironment of these residues could affect the coordinating interactions that hold the capsid units together. Another study demonstrated 4-log inactivation of a parvovirus, minute virus of mice MVM at 90 °C due to disintegration of the capsid [34]. While most studies use relatively high

temperatures to demonstrate temperature dependent virus inactivation, one study aimed to make mechanistic predictions on the effect of temperature on enveloped viruses at relatively low temperatures [131]. A dramatic five-tenfold increase in SARs CoV-2 decay was observed by increasing the temperature from 10 ºC to 27 ºC. However, when considering the effect of ambient temperature on the stability of viruses in the environment, other factors such as relative humidity must be considered simultaneously.

Relatively high pressures can dissociate oligomeric proteins of the virus capsid or the overall viral structure itself [35]. However, the extent of dissociation can vary dramatically between viruses belonging to different families as well as viruses belonging to the same family. One study showed the effect of pressure on three different viruses polio, rhino and foot and mouth disease (FMD) viruses, all belonging to the same family, *Picoroviridae* [35]. All three viruses possess an icosahedral capsid with 60 copies of four proteins, VP1 – VP4 [36-38]. The effect was largest on FMD virus, whereas polio and rhinoviruses were found to be stable at pressures under 2.4 kbar. The difference in the effect of high pressure on virus stability was attributed to the structural differences between the viruses. More specifically, the FMD viral capsid mass, the root means square thickness (rms) of the capsid proteins except VP4 and the thickness of the virus protein coat trimer are all much lower in comparison to polio and rhinoviruses.

Relative humidity is known to affect the size of the virus carrying aerosol and its aerodynamic behavior, therefore, dictating if a virus will stay suspended in air or deposit on a surface [39]. One study demonstrated that enveloped viruses show a higher chance of survival at lower levels of RH (< 50 %) due to the higher percentage of lipid content. Non-enveloped viruses on the other hand, were found to prefer relatively higher levels of RH (> 80%) [40]. At high RH, the presence of the lipid membrane can cause viruses to partition on the surface of aerosols and expose them to the air-liquid interface. The resulting surface tension, shear stress and hydrophobicity based conformational changes from the exposure can cause severe damage to enveloped viruses [41].

2.3.2 Surface properties

Adhesion of viruses to surfaces can depend on virus morphology, as discussed earlier, and properties of the surface being investigated [42]. Often, a combination of factors such as surface porosity, polarity (virus and surface charge), interacting forces (ex. electrostatic or van der waals) and hydrophobicity/hydrophilicity of the virus or the surface, dictate the ability of a viruses to persist and remain viable on surfaces [43].

A study demonstrated the ability of different surfaces (silica, nylon, stainless steel and polypropylene) to adsorb a human adenovirus (HAdV5) based on the polar and dispersive components of their respective surface tensions [44]. A large component of silica's surface tension is governed by the electron donor group. As a result, the interaction with HAdV5 was strongly repulsive (hydration pressure). Nylon is less polar than silica and has a relatively higher surface tension dispersive component, resulting in a much stronger attractive interaction (hydrophobic) between virus and surface. Stainless steel has a high electron acceptor component, resulting in strong polar interaction. Lastly,

Polypropylene (PP) is apolar and only viruses with dispersive components lower than that of water show attractive hydrophobic interactions with the surface. Comparison of the four surfaces based on surface free energies indicate, to promote virus adhesion, an overall low surface energy is favorable meaning (hydrophobic surfaces) whereas, to prevent virus adhesion, a high positive value of surface energy (hydrophilic surfaces) are preferred [42, 44]. Relative hydrophobicity of different viruses and their ability to wet surfaces also affects virus persistence. Viruses with hydrophobic proteins in the outer layer were found to favor hydrophobic surfaces for sorption.

Adhesion of viruses to surfaces further depends on porosity. Porous materials like cloth, and paper show low virus persistence, whereas non-porous, smooth surfaces such as glass, plastics and stainless-steel show higher persistence [42]. The titer of infectious Sars-CoV-2 was found to be reduced by (1.8-3.3) $\log_{10}$ $TCID_{50}mL^{-1}$ on printing paper and tissue paper in 30 min. The titers were reduced to undetectable values in 3 hours – 2 days. On non-porous materials, like banknotes and glass[45], infectious virus could be detected up to 7 days. Another common respiratory virus, influenza A virus, was found to persist 24-48 hours longer on low porosity surfaces such as stainless steel and plastic than porous surfaces [46]. The low persistence of viruses on porous surfaces may be associated to rapid drying of viruses on the surface. The size of a respiratory droplet carrying virus is reduced as it is absorbed by porous surfaces. In comparison, on non-porous surfaces, the water droplet leaves behind a thin, protective film of moisture providing enough resources to extend virus stability on the surface [47]. Enveloped viruses, as discussed earlier are more susceptible to desiccation and inactivation [42].

2.4 Tools for virus removal and inactivation

While maintaining good hygienic practices such as frequent washing of hands and avoiding crowded places are effective preventative measures to minimize exposure to infectious viral particles, other methods can be employed to control the spread of disease. The use of personal protective equipment and facial coverings have been reported as effective at reducing transmission and severity of disease [48-50]. Barriers are effective at reducing direct exposure to disease causing viruses, however, they do not inactivate them. Sanitization techniques are designed with the aim of inactivating viruses. Physical disinfection techniques such as heat and light, and chemical disinfection techniques using alcohols, sodium hypochlorite, surfactants and quaternary ammonium compounds can be used to inactivate viruses as well [51-57]. More recent developments include coating PPE and high frequency touch surfaces with antiviral agents to inactivate viruses and resolve the transmissible effects of virus persistence.

2.4.1 Physical barriers for virus removal (PPE, respiratory masks non-woven fabrics and filtration efficiency)

The purpose of physical barriers is not to inactivate or kill pathogens but to physically block common routes of entry such as the eyes, mouth, nose, and skin. The primary route of transmission for most respiratory viruses is the inhalation of aerosols carrying infectious viruses. Face coverings have been found to be 79% effective in

preventing transmission [58]. Non-woven materials such as polypropylene (spun bound or melt-blown), glass paper and woolen felt can be used in the production of personal protective equipment (PPE) and face coverings [59].

Melt-blown polypropylene fabrics are generated by depositing extruded molten polymer on to a conveyor through several small capillaries using pressurized hot air. A non-bonded, continuous web of fabric is created with a high filtration efficiency, high surface area to volume ratio, high porosity, and moderate mechanical strength [59]. Spun -bound polypropylene fabrics are produced in a similar manner. However, as the extruded molten fabric is deposited onto the conveyor as long thin filaments, weak bonds are formed between the overlapping fibers. This results in a much softer, less porous, stronger and more durable fabric [60]. Single use 3-ply and 4 ply non-woven polypropylene (PP) masks were utilized to combat the spread of COVID-19. A 3-ply mask consists of 3 layers, an inner layer to absorb moisture, a middle melt-blown layer to filter particulates, and an external hydrophobic layer to limit droplet deposition and entry. A 4-ply mask consists of an additional filter layer of activated carbon between the external most layer made of spun-bund fabric and the middle melt-blown filter layer [61]. Recent enhancements on masks explore the modification or functionalization of the filter media with antiviral agents [62]. QA compounds have demonstrated antiviral efficacy against a broad range of viruses. However, there is limited research coupling the antipathogenic property of QA compounds with the blocking properties of PPE to promote virus inactivation.

2.4.2 Physical inactivation techniques

Heat and light are common physical techniques employed to disrupt viral functionalities [63]. The choice of method used depends largely on the application. Heat can be used to denature thermolabile viral proteins while preserving the antigen. UV irradiation on the other hand can be used to preserve critical viral proteins which induce a host immune response [64].

Heat treatment is a widely used decontamination method for PPE, culture and transportation media, blood products etc. Numerous viruses including hepatitis, Influenza and parvoviruses show susceptibility for heat inactivation [65-67]. For viruses, in particular, heat denatures the secondary structures of proteins and other molecules, thereby impairing molecular function [68]. Viral protein and or genome undergo modification affecting their host-cell recognition and binding functions [57]. Virus inactivation rates can differ depending on dry or moist application of heat-based treatment procedures due to the effects brought in by evaporation and relative humidity [68].

Ionizing radiation such as x-rays and gamma rays can destroy viral genome but have little to no effect on other structural viral components: proteins and the membrane. Genetic damage occurs through radiolytic cleavage or by the action of free radicals on the genetic material [69].

11

UV irradiation to inactivate both single stranded or double stranded RNA or DNA viruses have been reported in literature. The antiviral effect and mechanism of inactivation also depend on the wavelength of incident light. High energy wavelength, UVC (200-280 nm), are the most potent while UVA (320-400 nm) and UVB (280-320 nm), being less energetic are non-ionizing and less potent. Inactivation with UV treatment occurs primarily by targeting the viral genome [69]. In the case of DNA viruses, pyrimidine dimers, more specifically thymine dimers form which can be lethal and mutagenic. The inactivation mechanism for RNA viruses differs as they contain uracil instead of thymine. UV irradiation results in photoproducts such as uracil dimers and cross-linking of RNA to proteins. However, damage to the viral capsid has also been reported [69]. UV irradiation, while one of the most commonly used disinfection techniques, often faces the challenge of non-linearity in terms of dose to lethal effect, as well as the inability to quantify the dose to be delivered [7].

2.4.3 Chemical inactivation techniques

Chemical disinfectants such as isopropanol, formaldehyde, hypochlorite solutions, hydrogen peroxide (H_2O_2), quaternary ammonium compounds (QACs) have been approved by the Food and Drug Administration (FDA) to sanitize surfaces and reduce the microbial load of surfaces [70]. Incorporation of metal ions into liquid disinfectants and sterilization techniques as potential antimicrobials has also been reported [71]. Numerous factors such as the type of disinfectant, treatment time, concentration and type of virus to inactivate should considered [54]. For example, for enveloped viruses, lipophilic disinfectants are advantageous. However, they do not work against non-enveloped viruses. An ideal disinfectant is quick, non-toxic, stable, and effective against a wide diversity of microorganisms [51].

Ethanol (>75%) and isopropyl alcohol (70 – 100%) are common alcohols, widely utilized in hospitals and laboratory settings to inactivate viruses [70]. Ethanol was found to inactivate both lipophilic and hydrophilic viruses by denaturation of proteins and cell membrane damage and lysis[32]. Isopropyl alcohol shows high potency against enveloped viruses containing a lipid membrane due to its lipid solvent properties.

Sodium hypochlorite is perhaps the most popular disinfectants used. Unionized hypochlorous acid can oxidize a variety of functional groups found on viral or cell proteins [53]. A 0.0005% solution of sodium hypochlorite showed a 4-log reduction titer of *Pseudomonas aeruginosa* PAO1 phage F116 by causing damage to the phage head, tail and overall capsid structure [72]. This particular property makes sodium hypochlorite an attractive disinfection strategy for disease causing non-enveloped viruses. However, the study reported no damage to the nucleic acid which limits the application towards non-enveloped viruses such as poliovirus which can be infectious just with their RNA [54]. While sodium hypochlorite is effective at low ppm levels, it is relatively harsh, has a strong odor and can irritate the mucous lining of the nose and mouth. Moreover, at low concentrations, the solution is not stable and loses is efficacy to environmental factors rapidly [73].

Quaternary ammonium compounds (QACs) belong to a class of cationic biocides and are frequently used domestically and commercially to meet daily disinfection needs. Structurally, QACs contain a positively charged nitrogen atom linked to three or four substituents with at least one double bond. Depending on the number of charged nitrogen atoms, QACs can be classified as mono-, bis- and multi- or poly-QACs. One of the substituents is constituted by a long aliphatic chain containing > 10 carbon atoms with an optimal chain length between 10-14 carbon atoms. The biocidal impact of QACs [55] may not necessarily depend on the number of charged nitrogen atoms but increase in the number of aliphatic chains is known to increase toxicity [74]. The antibacterial and antifungal function of QACs is well explored. However, a range of QACs have been demonstrated to show virucidal activity as well. Quaternary ammonium-based antimicrobials are known to inactivate a number of respiratory viruses. The biocidal activity is considered to a result of the disruption of the phospholipid membrane as in bacteria and fungi [75]. Lipid containing membranes are particularly susceptible to QACs due to their hydrophobicity [52]. A similar mechanism of inactivation is proposed for viruses. The alkyl chains of the cationic QACs can permeate the membrane, while the positively charged nitrogen atom can remain within the surface of the membrane. As a result, the virus can undergo severe changes in its physical and biochemical properties and the surface charge distribution [56].Ammonium chloride, a quaternary ammonium compound, was found to disrupt viral entry into the host by increasing the endocytic and lysosomal pH [76].

Hydrogen peroxide (H_2O_2), a well-known reactive oxygen species (ROS) which often finds domestic and therapeutic use as a strong antimicrobial agent. It is known to cleave or cross-link proteins, nucleic acids or lipids [54]. Any free sulfhydryl or double bonds can be potential targets for oxidation by the hydroxyl free radicals [55]. Liquid antiseptic applications of H_2O_2 are more common, however, dry decontamination applications have also been reported as effective for antimicrobial treatments. Concentrations of H_2O_2 varying from 0.5% to 13% have been reported to inactivate a broad spectrum of enveloped and non-enveloped viruses [54]. One study reported a 4 $\log_{10}$-reduction in the titer of HCoV 229E and poliovirus by treating the viruses with a 0.5% solution for 1 minute [77]. However, the study coupled the antimicrobial effect of H_2O_2 with ACCEL TB, as H_2O_2 by itself is quite unstable and loses efficacy rather rapidly. Regardless, H_2O_2 does provide certain advantages. Low concentrations of the biocide are required to achieve high reductions in LRVs with demonstrated efficacy against both enveloped and the more resistant non-enveloped viruses. Moreover, H_2O_2 degrades into oxygen and water, making it safe for the environment.

Heavy metals like silver (Au), gold (Ag), cobalt (Co), copper (Cu), Iron (Fe), titanium (Ti), and zinc (Zn), are able to interact with microorganisms. While the understanding regarding why certain metals or metal ions demonstrate antiviral properties is limited, it is known that several metal ions play a key role in critical metabolic processes of viruses such as the regulation of transcription/translation, protein folding/unfolding, and acid chaperoning. Certain metal ions such as zinc, copper and magnesium are also known to bind viral proteins [16]. An imbalance in these metal ions can therefore have detrimental effects on the survival of a virus. Several factors such as

the type of virus (RNA/DNA, single-stranded/double-stranded, enveloped/ non-enveloped), type of metal, concentration of the metal and the time of treatment all need to be considered in the design and development of metal based disinfection strategies [71].

Silver is particularly toxic to viruses which contain a sulfhydryl termini [78]. Binding to the functionality interferes with virus replication. Silver can also interfere with attachment of virus to the host cell surface. Antiviral activity of zinc oxide is similar to hydrogen peroxide [79]. The active oxygen species produced can damage the viral capsid and facilitate entry of more metal-ions into the virus. The virucidal property of copper is associated with its ability to alter its oxidation state and generate reactive oxygen species (ROS) under aerobic conditions via the Fenton and Haber-Weiss reactions [127]. These species can either disrupt the viral genome, proteins or the envelope, thereby affecting the integrity of the virus (figure 2.5) [80]. Changes in the molecular composition of viruses affect their ability to enter the host cell and leverage the host cell machinery to generate more infectious viral particles.

According to a study, copper and copper alloys reduced the titer of the enveloped coronavirus, HCoV 229E by fragmentation of the viral genome [80]. More significant role was played by copper ions. Another study compared the effect of copper ions on RNA/ DNA and enveloped/ non-enveloped viruses [71]. DNA containing, non-enveloped viruses ΦX174 and T7 were less sensitive to Cu (II) inactivation in comparison to RNA containing, enveloped viruses Φ6 and JV. The presence of RNA or lipid envelope may make the virus more vulnerable to inactivation by Cu (II). The role of copper ions vs ROS is influenced by the disinfection platform. A study of copper alloys (with varying percentages of brass) with the non-enveloped murine norovirus (MNV-1), showed as the copper content in the alloy decreased, ROS played a greater role in inactivation in comparison to Cu^{2+} [81]. In another study, the activity of Cu^{2+} was coupled with peroxide [71]. Copper ions alone were unable to inactivate the DNA containing enveloped HSV in 60 min. However, the application of a copper-peroxide mixture caused a 90% reduction in the titer of HSV in 15 min. Moreover, this inactivation was similar to other DNA containing enveloped viruses, ΦX174 and T7, despite the 5-fold and 50-fold difference in their diameter and genome size respectively.
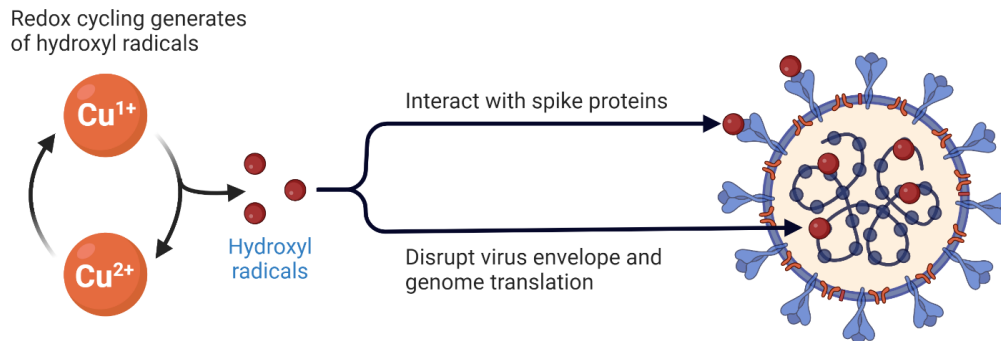
Figure 2.5: Interaction of hydroxyl radicals generated by Cu^{2+} with viral protein and genome; modified template "*Surfaces and SARS-CoV-2: A Spotlight on Copper*" from biorender.com.

2.4.4 Material enhancements for virus removal and inactivation

Physical and chemical modification of surfaces for improved hydrophobicity

Surface roughening is a common method used for improving the hydrophobicity of a surface [82]. Surface roughening can be achieved by chemical or physical modification using techniques of sublimation, laser micromachining, chemical vapor deposition. This step essentially helps increase the contact angle between the solid-liquid surface. While surface roughening by itself helps achieve high contact angles and thus high super hydrophobicity, roughening surfaces alone is not enough. Most machining processes are unable to impart complete and long-term super hydrophobicity. With time, these surfaces begin to lose their acquired super hydrophobic properties. A second step is thus required where a surface of interest is modified by coating it with low surface energy material. Since super hydrophobic surfaces are highly repellant towards water, low surface energy coating materials show similar properties as well [83]. Their low surface energies can be attributed to their non-polar chemistry (ex. CH_2/CH_3 or CF_2/CF_3) and close packing to create high contact angles (up to 120°) on their own. These materials can be adhered to a substrate of interest as a chemical modification. The two steps mentioned above can either be used one after another in a multi-step process of fabricating hydrophobic surfaces or used separately or together as a single step for fabrication [82].

Due to anti-staining, anti-wetting and self-cleaning (in extreme cases) of hydrophobicity, super hydrophobic surfaces enjoy great popularity across many diverse fields [84]. Non-woven fabrics commonly used in PPE are modified to impart high hydrophobicity to the outermost layer to reduce accumulation of virus load on the surface and enable recyclability. Coating regular surgical masks with graphene increased the contact angle to 110° [85]. A different study sought to suppress airborne and fomite

15

transmission by using a superhydrophobic silanized silica nanoparticle-based coating on common surfaces such as copper, glass, PPE, steel and plastic [86]. Significantly reduced viral activity (99.997 – 99.99995) was observed on the coated surfaces.

Metal-based nanoparticles

Metal based nanoparticles have gained tremendous recognition as efficient antiviral tools. Nanoparticles, by definition, have at least one of three dimensions in size < 100 nm. As the diameter of the particles decreases, the total surface area available for application increases [87]. The three methods, chemical, physical and biological methods used to generate nanoparticles allow tight control over the size, shape and structural composition of the final product [88]. Numerous metal nanoparticles with virucidal activity such as gold, silver, copper, zinc and iron have been reported [89].

Silver nanoparticles (AgNPs) bring about an antiviral effect by inhibiting virus infection at an early stage, either by preventing virus attachment or entry into the cell [90, 91]. The virucidal behavior of AgNPs against HIV-1 was found to be due to the binding of silver with one of the structural proteins, gp120 which facilitates binding of virus to the host cell [92]. Nanocomposite coating of with poly(methyl methacrylate) embedded with Cu and CuO nanoparticles significantly reduced the titer of HCoV-OC43 and lentivirus, both enveloped viruses. The inactivation was hypothesized as a result of the direct contact of viruses with the nanoparticles which had been previously reported for Cu in literature [93]. Zinc oxide nanoparticles showed H1N1 influenza virus inhibition by as much as ~95%. Like AgNPs, ZnO NPs also work by preventing entry of virus into the host cell [94]. In the case of SARs CoV-2, ZnO NPs disrupted viral entry into CCD-19 Lung human lung fibroblasts by interacting with the ACE 2 receptor [95]. A 2 pg/mL solution of iron oxide NPs and infected media showed an 8-fold reduction in the viral RNA of influenza virus after 72 hrs [96]. The interaction of the iron nanoparticles with exposed sulfur bearing viral protein knobs could inhibit binding and entry of the virus into the host cell. Despite the numerous applications of NPs in virucidal materials. NPs carrying metals have been reported to show toxicity towards human cells due to lipid peroxidation, disruption of cell membrane, inflammation etc. Therefore, it is extremely important to thoroughly evaluate not only the antiviral effect but also the cytotoxic effect of these novel metal nanoparticles.

Clay minerals

The interaction of viruses with clay minerals has been widely studied. The interactions depend on electrostatic surface charge and sorption properties of the minerals. [97]. The large surface area of the clay minerals, adsorption capacity, large ion exchange capacity, thermal and chemical stability, biocompatibility, low toxicity, and relative abundance also make them attractive candidates to be used as polymer composites for virucidal agents like metal ions and metal nanoparticles.

Kaolin, bentonite, vermiculite and sepiolite are common clay minerals that find application as additives or fillers in paint or ingredients in pharma [98]. Bentonite, a

montmorillonite mineral, due to isomorphous substitution, carries a net negative charge and shows high cohesive affinity towards viruses like SAR CoV-2 and polioviruses with positive sense RNA genomes. An environmentally sustainable paste with bentonite was found to absorb 99.99% and 95% or SARs-COV-2 and poliovirus, respectively [99]. Another study reported the reduction of the total amount of influenza virus by log 3 and log 5, respectively, upon treatment with silver and copper oxide NP infused kaolin.

There is abundant literature demonstrating the antiviral efficacy of nanoparticle-based clay mineral platforms. However, the implications of long-term use and accumulation of nanoparticles in the environment are unknown. There is therefore a need to explore suitable alternatives with the more sustainable metal ions. Vermiculite and sepiolite are both phyllosilicate minerals, composed of tetrahedral and octahedral layers with chemical formulas $(Mg, Ca)_{0.3-0.45} \cdot (H_2O)_n(Mg, Fe, Al)_3(Al,Si)_4O_{10}(OH)_2$ and $Mg_4Si_6O_{15}(OH)_2 \cdot 6H_2O$ respectively. Vermiculite is characterized by a dry and flaky physical appearance whereas sepiolite has a more talc like, fibrous structure. Both clay minerals display great potential for displacement of the constituent Mg^{2+} ions with a more potent, antiviral metal ion such as Cu^{2+}. However, no research yet provides insight into the use of such an antiviral platform to regulate disease transmission.

In summary, the physical and biochemical properties of viruses can be exploited to design virucidal materials to control both the direct and indirect transmission of viruses. A large number of virus disinfection techniques have already been developed to mitigate the spread of infectious viral diseases. However, conventional approaches employing PPE and facial coverings only provide a physical barrier between the pathogen and human host. They do not reduce the environmental viral burden which is a concern since numerous viruses are able to remain viable and infectious for prolonged periods of time. Physical (heat and light) and chemical (alcohols, sodium hypochlorite, QACs, and metal ions) disinfectants either need external stimuli for inactivation or use harsh active agents at concentrations that pose a danger to both human health and the environment. The novel virucidal materials described in this thesis seek to couple the physical blocking property of PPE with virucidal agents in low concentrations to inactivate a broad spectrum of disease-causing viruses. Magnesium ions are displaced with the antiviral cupric ions in naturally occurring clay minerals. These clay minerals often find use as fillers in polymer composites to coat high frequency touch surfaces. The application can thus be used to control fomite-based transmission of viruses. Similar applications using metal nanoparticles have been reported, however, the implications of long-term use and accumulation of nanoparticles in the environment are unknown. The second and third studies modify the surface of non-woven fabrics used in facial coverings and PPE with potent antiviral agents such as quaternary ammonium compounds and hydrogen peroxide generating 6-hydroxydopamine. Both coatings seek to reduce the accumulation of viruses on the surface of mask, improve recyclability and reduce environmental waste.

3   Materials and Methods

3.1 Cells and viruses

3.1.1 Cell maintenance

Porcine kidney cells (PK-13, ATCC) used as the indicator cell line for porcine parvovirus were cultured in Eagle's minimum essential media (EMEM, Thermofisher scientific) supplemented with 10% v/v fetal bovine serum (FBS, Thermofisher scientific) and 1%v/v pen/strep (Invitrogen). Cells were split at 70% confluency (every 2-3 days) at a 1:5 ratio and incubated at 37 °C with 5% CO_2 and 100% humidity.

Human Lung Fibroblasts (MRC-5, ATCC) cells used as the indicator cell line for human coronavirus strain 229E were cultured in Eagle's minimum essential media (EMEM, Thermofisher scientific) supplemented with 10% v/v fetal bovine serum (FBS, Thermofisher scientific), 1% v/v pen/strep (Invitrogen), 1% v/v 100mM sodium pyruvate (Thermofisher scientific), and 1% v/v non-essential amino acid (MEM NEAA, Thermofisher scientific). The MRC-5 cells were inoculated at a seeding density of 2 x 10^4 cells /cm^2 at a ratio of 1:5, incubated at 37 °C with 5% CO_2 and 100% humidity and were split every 2-3 days (or when 70% confluent).

Bovine Turbinate cells (BT, ATCC CRL 1390) cells used as the indicator cell line for bovine diarrhea virus were grown in Dulbecco's Eagle's minimum essential media (DMEM) supplemented with 1% v/v penicillin–streptomycin, 1% v/v 100mM sodium pyruvate and 10% v/v FBS at 37 °C with 5% CO_2 and 100% humidity and split every 3-4 days or at 70% confluency.

Vero cells (ATCC CCL-81) were used as the indicator cell line for suid herpesvirus-1. The cells were grown in Eagle's minimum essential media (EMEM) supplemented with 1% v/v penicillin–streptomycin and 10% v/v FBS at 37 °C with 5% CO_2 and 100% humidity and split every 2-3 days or at 70% confluency.

3.1.2 Virus propagation and titration

Porcine parvovirus (PPV), generously provided by Dr. Carbonell's lab (North Carolina State University) was propagated in PK-13 cells. Breifly, PPV was added at a concentration of 10^3 MTT_{50}/mL (diluted in 1X PBS pH 7.2, 3% FBS, 1x pen/strep) to PK-13 cells seeded (6 x 10^5 cells /flask) and grown overnight. After adsorbing the virus for 1.5 hours at low-speed rocking, 9 mL of fresh media was added to the infected cells and incubated at 37 °C till 100% cytopathic effect (CPE, 4-6 days) was observed. The virus was harvested, using two freeze-thawed cycle, and cells scrapped into the media. The suspension was collected in a 15 mL conical low binding tube, and centrifuged (ThermoScientific Sorvall ST16R Centrifuge) at 5000 rpm for 15 minutes at 4°C. The PPV supernatant was collected and stored at -80°C with 10% v/v glycerol until used.

Human Coronavirus (HCoV 229E, BEI Resources), 1 mL was added to a 70-80% confluent monolayer of MRC-5 cells (culture media drained and monolayer washed with

1X PBS, pH 7.2) at a concentration of 10^4 MTT_{50}/mL. The viruses were adsorbed for 1.5 hours by low-speed rocking on a gyratory shaker. After adsorption, 9 mL of fresh media (complete EMEM media described earlier for MRC5, supplemented with 2% FBS instead of 10% FBS) was added to the infected cells. Infected HCoV 229E flasks were incubated at 35 °C, 5% CO_2 and 100% humidity until 100% CPE was observed (2-3 days). On the day of 100% CPE, the infected flasks were freeze-thawed twice. The suspension for each was collected and centrifuged at 5000 rpm for 15 minutes at 4°C. HCoV supernatant was collected and stored at -80°C with 10% v/v glycerol.

Suid herpesvirus 1 strain Aujeszky (SuHV-1, ATCC VR-135),was propagated similarly. Following 100% CPE, the virus was subjected to two freeze-thaw cycles and harvested by centrifugation at 5000 rpm for 5 min. The supernatant was collected and stored -80 °C in 10% (v/v) solution of DMSO.

For, Bovine viral diarrhea virus 1 (BVDV, ATCC VR-1422) was propagated. Following 100% CPE, the virus was subjected to two freeze-thaw cycles and harvested by centrifugation at 5000 rpm for 5 min. The supernatant was collected and stored -80 °C in 10% (v/v) solution of DMSO.

The colorimetric MTT cell viability assay determined the titer of infectious virus [100]. Briefly, PK-13 cells were seeded at a cell density of 8 x 10^4 cells/ml and MRC5-cells at 1 x10^5 cells/ml in 96-well plates for 12-24 h. Virus supernatant (25μL) was added to the wells in quadruplicate, with a serial dilution of 1:5 across the plate. After incubating the plates for 6 days at 37 °C (PK-13) and 35 °C (MRC-5), MTT (3-(4,5-Dimethylthiazol-2-yl)-2,5-diphenyltetrazolium bromide) at a concentration of 5 mg/mL in PBS, pH 7.2, (Thermofisher Scientific) was added to the wells for 4 hours. Then, 10% Sodium dodecyl sulfate (SDS, catalog number) was added to the wells as a solubilization buffer. After 4-24 hours, the absorbance was determined using a Synergy Mx microplate reader (BioTek, Winoski, VT) at 550 nm. The 50% infectious dose of the virus was determined by finding the concentration where 50% of the cells were viable, labeled the MTT_{50}. Log reduction values (LRV) were calculated using equation (3.1).

$$\text{Viral titer} = -\log_{10}\frac{Ci}{Cf} \qquad (3.1)$$

where C_i and C_f are initial and final concentrations, respectively.

3.2 Cupric-ion infused clay minerals

3.2.1 Preparation of clay minerals

Vermiculite (Virginia vermiculite LLC) or sepiolite (IMV Nevada) powders were prepared as described [101]. Briefly, the powders were dried in oven at 105°C for 24 hours. Weighed 5.00 g of dried powder was dispersed in 100 mL of 0.2M CuSO4·5H2O solution, prepared with distilled water. The suspension was heated to 80°C and blended with a magnetic stirrer continuously for 3 hours. Suspension cooled to room temperature was filtered with #1 filter paper. The filter cake was washed with 50 mL distilled water

three times. The final cake was dried at 105°C for 24 hours, then re-ground into powder. The clay minerals were prepared by Dr. Bowen Li's research group from the Materials Science and Engineering department at Michigan Technological University.

3.2.2 Characterization of vermiculite and sepiolite with FE-SEM

The samples were imaged using a Hitachi S-4700 Field Emission Scanning Electron Microscope (FE-SEM). Before imaging, 0.02g of loose vermiculite and sepiolite powders were incubated with either 1 mL PPV at a concentration of 10^7 MTT_{50}/mL or a mock buffer for 2 hrs at 4 °C in 360° rotation motion. Following incubation, samples were pelleted, by centrifugation (10,000 rpm, 15 min) and supernatant removed. The virus was cross-linked to avoid infectious virus being used in the microcopy facility. Pelleted samples were re-suspended in 1 mL solution of 0.025 M HEPES buffer containing 7.14 uL of 70% glutaraldehyde and incubated for 1 hr at room temperature. Following cross linking, samples were pelleted by centrifugation, the supernatant was removed, and the pellet washed with HEPES buffer to remove residual glutaraldehyde.

Samples were stained with 2% uranyl acetate solution and then dried in a fume hood overnight. The following day, the dried powder was applied to a carbon tape-coated pin mount. A compressed air can was used to remove any loose particles. A Cressington 208HR Sputter Coater was used to coat the sample with a 2.5 nm film of iridium, which improved the sample conductivity to prevent charging under the FE-SEM. While being imaged under the FE-SEM, an accelerating voltage of 3 kV, a condenser lens setting of 12, an emission current of 7 eV, and a working distance of 3 mm were used.

3.2.3 Evaluating antiviral efficacy of clay mineral powders

Loose powder (0.02 g) was added to 1 mL (2% w/v) of PPV or HCoV (6 $\log_{10}$ MTT_{50}/mL) in low-binding microcentrifuge tubes. The solution was incubated at 4°C in a 360° rotation motion. After incubation, the clay minerals were separated from the virus suspension by centrifugation (10,000 rpm for 15 min). The supernatant was collected and stored at 4°C until titrated.

3.2.4 Mechanism of virus inactivation

ICP testing:

For inductively coupled plasma (ICP) testing, the 0.2wt% suspensions of each clay mineral samples were prepared with 0.025 M HEPES solution, PBS (1X, pH 7.4) or distilled water. The samples were incubated for 2 or 24 hours as previously described. Following incubation, the samples were centrifuged (10000 rpm for 15 min) and supernatants separated and tested for the amount of metal ions released.

EDTA testing:

Etheylenediaminetetraacetic acid (1 mM EDTA, catalog number) was added to PPV solution. Three different cases were considered. In case 1, EDTA was added to the virus solution before incubation (pre-EDTA). In case 2, EDTA was added to the virus-

clay suspension after incubation (post-EDTA). Lastly, in case 3, no EDTA was added (No-EDTA). HEPES solution (25 mM) was used as the mock buffer in the no-EDTA case to ensure volume consistency between the three cases. At the end of the incubation period, the supernatant containing treated PPV was separated from the powders by centrifugation (10000 rpm for 15 min) and titrated.

BSA testing:

Bovine serum albumin (BSA, catalog number) at a 1% concentration was either added or not added to the virus-clay suspension prior to a 2 hour incubation period. Following incubation, clay mineral powders were separated from the virus solution by centrifugation (10000 rpm for 15 min) and the supernatants containing the treated PPV and HCoV were titrated.

3.3 C_{12}-benzophenone functionalized melt-blown and spun-bound polypropylene fabrics

3.3.1 Polymer synthesis and characterization

The C_{12}-quaternized benzophenone, N-(4-Benzoylbenzyl)-N,N-dimethyldodecan-1-aminium bromide (QA1) was prepared as described [102] with the reaction scheme shown in figure 3.1. Briefly, 4-(bromomethyl)benzophenone and *N,N*-dimethyldodecylamine were dissolved in isoamyl alcohol. The vessel was tightly sealed and heated to 95 °C in a heating block. Following heating and stirring for 24 hours, the vessel containing the mixture was cooled to room temperature. The solution was concentrated and a waxy solid mixture was obtained which was dissolved in methylene chloride and recrystallized. Vacuum filtration followed by drying for 18 hours yielded the pure product as a white solid.
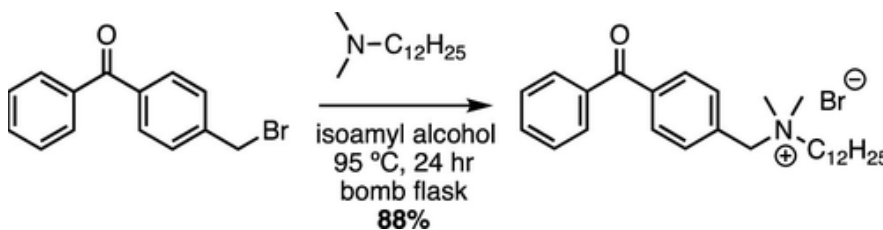
Figure 3.1: Scheme 1. Synthesis of Compound QA1[102]. Figure reprinted from reference # 102, Copyright 2022, Sorci et. al., published under license CC BY-NC-ND 4.0.

Poly(1-dodecyl-4-vinyl pyridinium bromide (QA2) was prepared as described [102] with the reaction scheme shown in figure 3.2. Poly(4-vinyl pyridine) and 1-bromododecane were dissolved in acetonitrile and ethanol and heated to reflux for 96 hours. The resultant solution mixture was cooled and concentrated to obtain a viscous brown oil. This viscous semi-solid solution was dissolved in hot ethanol and precipitated by adding dropwise into cold acetone. Lastly, centrifugation was used to isolate the precipitate to obtain the final product as a white powder.
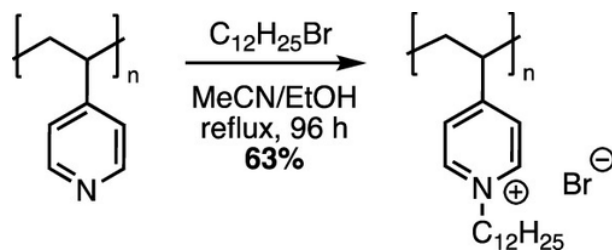
Figure 3.2: Scheme 2. Synthesis of Compound QA2 [102]. Figure reprinted from reference # 102, Copyright 2022, Sorci et. al., published under license CC BY-NC-ND 4.0.

3.3.2 Covalent grafting and physisorption to filtration media

Compound QA1 was grafted and compound QA2 was physisorbed onto mbPP and sbPP non-woven fabrics as described [102]. Briefly, for QA1 grafting, 150 µL of the solution was drop-cast onto fabric swatches. The solvent was evaporated followed by UV irradiation for 10 min per side. Sonication of swatches in excess acetone removed unbound material from the fiber surfaces. Finally, the swatches were dried for 1 hr under vacuum. Compound QA2 was physisorbed by completely immersing the mbPP and sbPP filters in isopropanol solution for 15 min at room temperature while rocking on an orbital shaker. The filters were washed by dipping in clean isopropanol (3X) for at least 30 s each followed by drying at 70 °C for 1 hour.

3.3.3 Antiviral test against SuHV-1 and HCoV 229E

Prior to the antiviral test, the fabrics were treated with isopropanol (70%) phosphate buffered saline (PBS, 1X pH 7.2) to promote their wetting properties and virus attachment as shown in figure 3.3. Swatches (1 cm x 1cm) were disinfected with isopropanol and gently washed twice with 30 mL of PBS (1X, pH 7.4). Viral stocks (6 $\log_{10}$ MTT$_{50}$/mL) were applied to the QA1 and QA2 modified and bare mbPP and sbPP in multiple small droplets (5 µL each) and allowed to dry. The samples were then gently washed with a small volume of PB (1X, pH 7.0) to remove unbound virus if any, and then vortexed vigorously in a larger volume (1.3 mL) of EMEM buffer containing 1% bovine serum albumin (BSA) to elute bound virus (figure 3.3) [102]. The virus samples recovered during the wash and elution steps were titered.
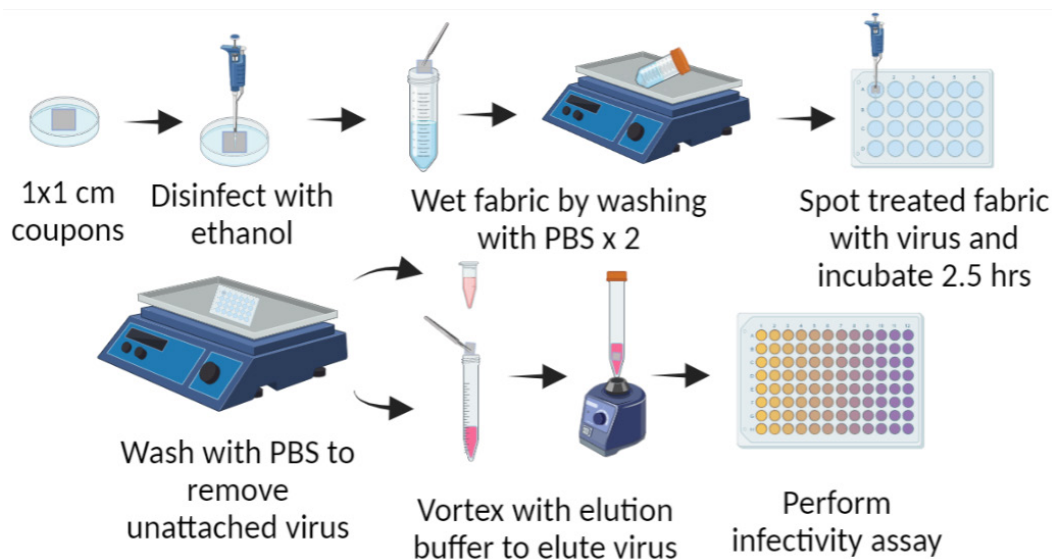
Figure 3.3: Wash step with PB w/o saline and Elution step with 1% BSA in complete EMEM media for cell culture; figure created in biorender.com.

3.4 Catechol coated melt-blown polypropylene fabrics

3.4.1 Preparation and characterization

Acrylic acid N-hydroxysuccinimide (AA-NHS) and acrylamide (AAm) were copolymerized through free radical polymerization and further reacted with 6-OHDA to obtain the final copolymer (AA-DA-OH)-co-AAm as shown in figure 3.4. Polyacrylamide (pAAm) as synthesized in figure 3.4 a was used as the control coating. The fabric (mbPP) was soaked in 5 wt% copolymer solution with and without the catechol group in dimethyl sulfoxide for 1 h. The volume of the polymer solution was adjusted to obtain 30 and 40 wt% polymer coatings on the fabric.

Proton nuclear magnetic resonance (^{1}H NMR), and UV-vis spectroscopies were used to characterize the composition of the polymer. The morphology of the polymer-coated PP fabric was determined using field emission scanning electron microscopy (FESEM). The porosity of the polymer-coated PP was evaluated using the n-butanol uptake method [103]. The generation of H_2O_2 from the coatings after hydration by 100 μL PBS (1X, pH 7.4) was determined by using quantitative Ferrous Oxidation-Xylenol orange (FOX) assay [104].
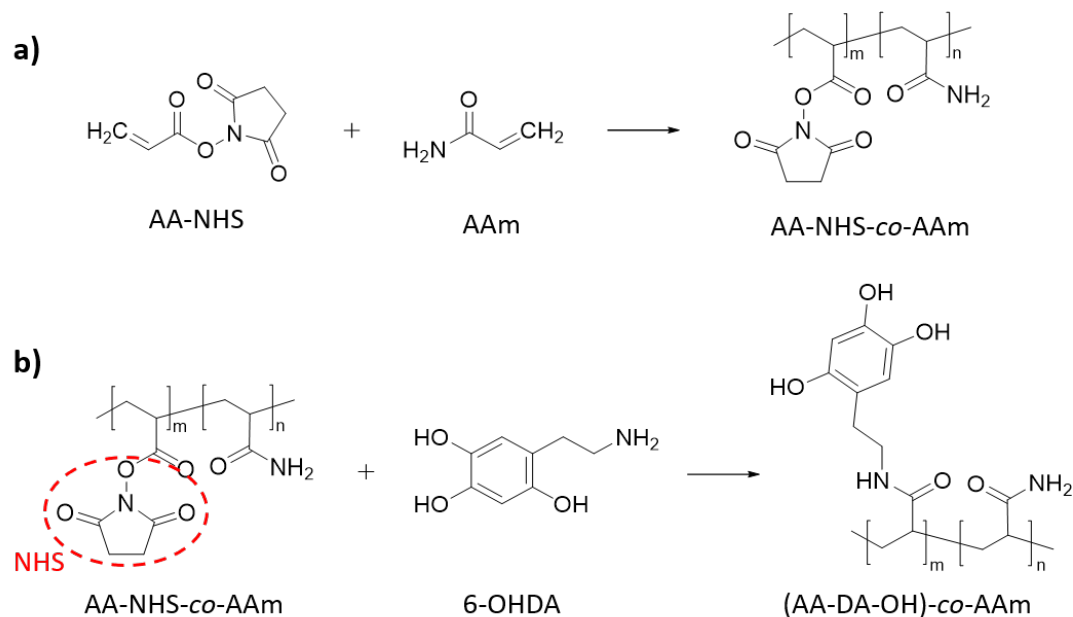
Figure 3.4: Two step 6-OHDA-based polymer synthesis. a) synthesis of NHS-containing copolymer (AA-NHS-co-AAm) by using acrylic acid N-hydroxysuccinimide (AA-NHS) and acrylamide (AAm) b) NHS in the AA-NHS-co-AAm further reacted with 6-OHDA to prepare 6-OHDA-based polymer (AA-DA-OH)-co-AAm. Polymer synthesis completed and figure provide by Fatemeh Razaviamri

3.4.2 Virus inactivation and kinetics

Prior to virus treatment, circular swatches of the control and catechol coated fabrics were cut to fit the wells of standard cell culture compatible, sterile, 24-well plates. The fabrics were then disinfected by UV for 15 minutes in a biosafety level -2 cabinet. Following disinfection, a single 150 μL drop of at least 6 $\log_{10}MTT_{50}$/mL solution of HCoV or BVDV was added to each of the fabrics and incubated for 1, 2, 6, or 24 hours as shown in figure 3.5. Following incubation, the treated virus droplet was carefully recovered and titrated.
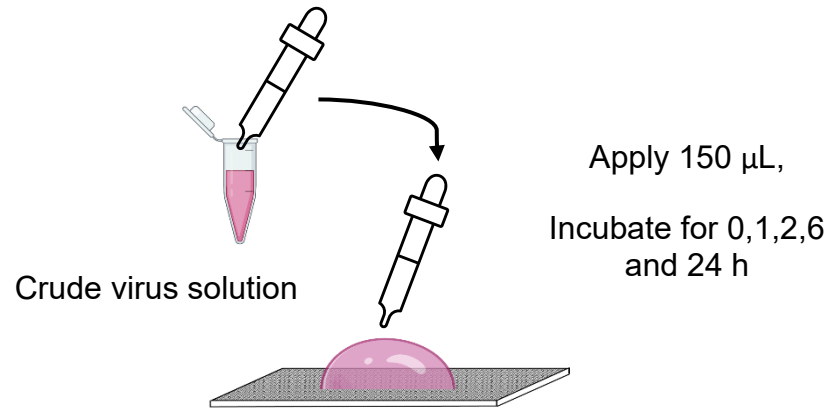
Figure 3.5: Incubation of crude virus solution of HCoV or BVDV with bare and polymer coated non-woven melt-blown PP; figure created in powerpoint.

4 Results

4.1 Cupric-ion infused clay minerals

The use of copper as an effective antimicrobial agent is well established. The first biocidal use of copper dates to 2600 B.C. by the Egyptians to decontaminate drinking water and treat chest wounds. Evidence of frequent use of copper by physicians has also been recorded in the De-Medicina [105]. More recent advancements report the important role ionic and metallic copper play in various alloys, nanomaterials, and polymer composites to impart biocidal properties to them [81, 93, 106]. The antiviral activity of copper, in particular, is associated with its ability to alter its oxidation state to generate copper ions (Cu^+ & Cu^{2+}) and reactive oxygen species (ROS), which can either disrupt the viral genome, proteins or the envelope, and affect the integrity of a virus [80]. Changes in the virus molecular composition can alter their ability to enter the host cell and leverage the host cell machinery to generate more infectious viral particles. Targeting these viral components is therefore crucial to inactivating viruses and mitigating disease transmission.

With a deeper understanding of the virucidal effect of copper, and a recent surge in highly transmissible viral diseases, there is renewed interest in utilizing copper as a platform for controlling disease spread. Disease transmission can occur directly, by the inhalation of airborne aerosols or large droplets carrying infectious viruses, or indirectly by encountering pathogen contaminated surfaces (fomites) [6, 9, 50]. Boosting immunity through increased vaccination efforts is perhaps the most effective, preventative measure to control disease transmission. However, development of supplementary strategies, employing surfaces with virucidal properties or high affinity for virus adsorption, to rapidly remove and inactivate viruses has gained tremendous attention [16, 93, 94]. This study presents the use of a strong antiviral agent, cupric ions (Cu^{2+}), in highly adsorptive clay minerals, vermiculite and sepiolite.

Layered silicate minerals are often used in a variety of polymer composites as cost effective fillers to enhance their physical and mechanical properties. They improve thermal stability, tensile strength and gas/water permeability [107]. Naturally occurring clay minerals also find use in medicine. Smectite, kaolinite, palygorskite have been used to adsorb and remove suspended toxins (organic matter) through consumption or topical application [108]. Sepiolite has been used in drug delivery systems [109].

Vermiculite and sepiolite are both phyllosilicate minerals, composed of tetrahedral and octahedral layers of silica and alumina. Vermiculite is characterized by a dry and flaky physical appearance [110]. Sepiolite has a more talc like, fibrous structure [111]. Clay minerals are used as carriers of metal nanoparticles such as Au, Ag, Cu, and Zn due to their large cation exchange and high adsorption capacity [98]. However, the implications of the long-term use and accumulation of nanoparticles in nature are unknown. Our study eliminates the need for nanoparticles altogether. Instead, a well-established platform for inactivating viruses, cupric ions (Cu^{2+}), were directly incorporated into clay minerals.

The motivation of the study was to develop a novel virucidal material with the potential to mitigate spread of disease which occurs through fomite transmission. The ability of clay minerals to adsorb viruses is coupled with copper, a strong antimicrobial agent, to remove viruses from surfaces and potentially inactivate them considerably. A series of experiments were performed to demonstrate time-based inactivation efficacy of Cu^{2+} infused powders against the non-enveloped porcine parvovirus (PPV) and the enveloped human coronavirus (HCoV-229E). A surface attachment and contact-based virus inactivation mechanism was hypothesized by performing a series of ion release and surface blocking experiments.

4.1.1 Infusion of vermiculite and sepiolite with cupric ions (Cu^{2+})

Two clay mineral samples, vermiculite and sepiolite, were modified by treatment with $CuSO_4$. The high sorption and cation-exchange capacity of the minerals were leveraged to displace magnesium ions (Mg^{2+}) from the clay matrix with Cu^{2+}. The procedure lacked a high temperature reduction step to ensure the incorporation of copper in its ionic form instead of metallic copper, as previously reported [112]. X-ray diffraction (XRD) was used to confirm incorporation of Cu^{2+} into vermiculite and sepiolite clay mineral samples.

4.1.2 Treatment of clay powders containing Cu^{2+} with non-enveloped and enveloped viruses

The ability of the Cu^{2+} containing vermiculite (V-Cu and UnV-Cu) and sepiolite (S-Cu) clay mineral powders to reduce viral burden was evaluated against the enveloped human coronavirus (HCoV 229E) and the non-enveloped porcine parvovirus (PPV). In addition to the differences in their molecular composition, the two viruses also differ significantly in size with PPV being ~ 20 nm and HCoV ~120-200 nm in size [130, 102]. HCoV was also used as a safer alternative to SARs CoV-2. It also acted as a model for other enveloped viruses that remain infectious on surfaces for prolonged periods of time [30]. Untreated vermiculite (V) and sepiolite (S) samples were used as negative controls. Powdered cuprous oxide (Cu_2O) was used as a positive control to quantitate the efficacy of the novel powders as potential antiviral materials. Cu_2O makes a suitable positive control as it demonstrates virucidal activity against a broader spectrum of viruses such as influenza virus, herpes simplex virus, and bacteriophages, in comparison to cupric oxide (CuO) [113]. A list of the unmodified and modified samples tested in this study are tabulated in table 4.1.

Table 4.1: Summary of clay mineral powders used in the antiviral study

Sample	Abbreviation	Notes
Vermiculite	V	Negative Control
Unexfoliated vermiculite infused with Cu^{2+}	UnV-Cu	Smooth, dense flake layers [110], similar to native powder
Exfoliated vermiculite infused with Cu^{2+}	V-Cu	Porous, irregular with numerous air layers
Sepiolite	S	Negative Control
Sepiolite infused with Cu^{2+}	S-Cu	Talc-like, fibrous structure [111], physical properties similar to the native powder
Cuprous Oxide	Cu_2O	Hydrophobic, insoluble, and difficult to get into suspension

The ability of Cu^{2+} containing clay minerals to reduce the titers of both PPV and HCoV in 4 hours is shown in Figure 4.1A and B. V-Cu and UnV-Cu reduced the viral titer of PPV by a log reduction value (LRV) of 2.6 ± 0.4 and 2.5 ± 1.0 $\log_{10} MTT5_0$/mL as shown in figure 4.1A. Log reduction value (LRV) is a standard measure for how effectively a certain substance reduces the load of a given pathogen. Mathematically, an LRV of 1 is equivalent to reduction of pathogenic load by 90%. Against HCoV, the performance of UnV-Cu was significantly superior to V-Cu (p-value=0.008) as observed in figure 4.1B UnV-Cu showed 2.5 ± 0.7 $\log_{10}$-reduction in HCoV titer in comparison to < 1.0 $\log_{10}$-redcution observed with V-Cu. Exfoliation of the vermiculite powder could cause Cu^{2+} to be in the deep layers and pores of the powder, restricting the access of the much larger HCoV (~200nm) to Cu^{2+} ions. However, PPV being relatively smaller (~20 nm), and comparable to the pore size of vermiculite could readily access the Cu^{2+} rich sites in the exfoliated powder. Moreover, the inability of the negative control powder, V, to reduce the titer of PPV or HCoV suggests that Cu^{2+} ions impart antiviral properties to the exfoliated and unexfoliated vermiculite powders.

S-Cu showed 3.5 ± 0.2 and 3.2 ± 0.0 log10-reduction in the titers of PPV and HCoV, respectively, as seen in figure 4.1A and B. Interestingly, the control powder, S also showed a considerable reduction in the viral titers of both the viruses suggesting the ability of the control to either reduce viral load due to insufficient binding, inactivation or insufficient recovery of the incubated virus sample from the mineral powder. Sepiolite displays a talc-like, porous and fibrous morphology. There is a possibility for entrapment of virus particles in the pores or between the powder particles in the clay pellet formed during centrifugation. Regardless, Cu^{2+} containing sepiolite showed significantly more reduction in the viral titer than the control powder (p value = 0.002, per a student t-test).

The positive control, Cu$_2$O, showed results comparable to UnV-Cu and S-Cu against HCoV (p value > 0.1). However, efficacy against PPV was limited (LRV < 1 log$_{10}$-reduction), at least at 4 hours post incubation. Non-enveloped viruses, in general, are more difficult to inactivate as they lack the lipid bilayer [114]. The ability of these novel clay minerals to remove non-enveloped viruses, is therefore, a rather significant finding.
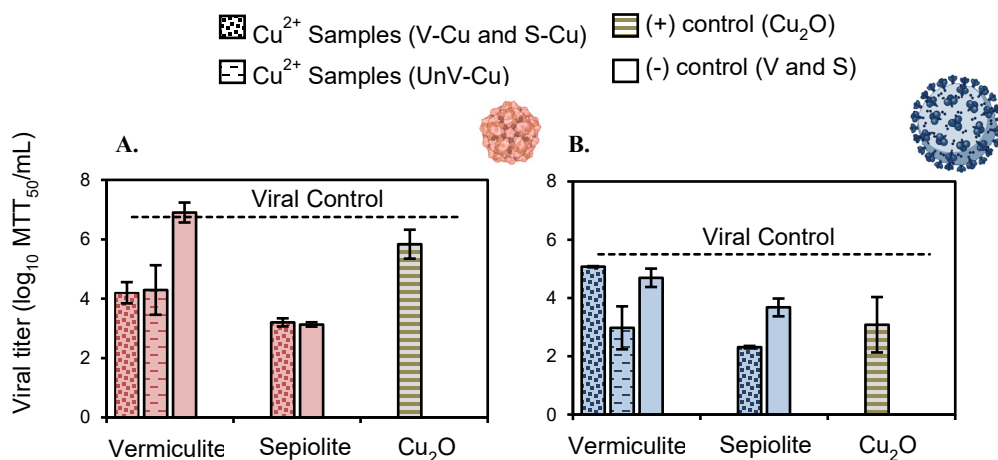
Figure 4.1: Viral titers observed after incubation of 2% (w/v) control and Cu^{2+} containing clay mineral powders with 1 mL of 6 log$_{10}$ virus solution in 360° rotatory motion for 4 hours at 4 °C. **A*.** PPV **B.** HCoV. The dashed line represents viral control.

 *Data collected by Vaishali Sharma

Overall, the results suggested Cu^{2+} imparted antiviral properties to the clay minerals potentially through inactivation or removal (adsorption) of viruses. More interestingly, the ability of these mineral powders to reduce the titer of PPV, a more resistant virus due to the lack of a lipid bilayer, is noteworthy. The use of these clay minerals could potentially be extended to the inactivation of numerous other non-enveloped viruses known to cause diseases in humans such as noroviruses (dysentery), rhinoviruses (common cold) and polioviruses (polio). Additionally, it is also important to note that the inactivation results presented here are for a worst-case scenario as the studies were performed at a rather low incubation temperature of 4 °C. These same studies may yield higher reductions in viral titers if repeated for incubation temperatures higher than the one tested.

4.1.3 Kinetics of virus removal

Cupric ion containing novel powders displayed potential antiviral activity against both PPV and HCoV 4-hours post incubation. Next, a kinetics study was performed to establish a relationship between the amount of virus removed with the incubation time for

a fixed concentration of Cu^{2+} containing powder (2% w/v). Each of the Cu^{2+} containing and control mineral powders were incubated with 1 mL of at least 6 $\log_{10}$ MTT_{50}/mL virus solution, as previously described. PPV was incubated for 1, 2, 4 and 24 hours and HCoV 229E for 15 min, 30 min, 1, 2, 4 and 24 hrs. Since enveloped viruses are more susceptible to inactivation, lower time points were considered in the kinetics study for HCoV 229E.

A general trend was observed where the viral titer was reduced as the incubation time was increased (figure 4.2A and 4.2B). Following 2-hours post incubation, the viral titers of PPV and HCoV were reduced by 2.6 and 2.4 $\log_{10}$ respectively by UnV-Cu. This corresponds to about 99.9% reduction in the viral load. V-Cu displayed a different antiviral profile depending on the virus model. After 2 hours of incubation, LRV of 0.8 $\log_{10}$ was observed for the enveloped model, HCoV. However, for the non-enveloped model, LRV > 3 $\log_{10}$-reduction was observed. Negative control, V continued to show no effect on the virus over the course of the experiment for either of the virus models. S-Cu showed 3.4 and and 3.5 $\log_{10}$-reduction of PPV and HCoV respectively. As observed in the single time-point study, S reduced the titer of both the viruses with increasing time. This may appear to be "significant virus removal". However, it is difficult to conclude if this reduction in viral titer is a result of inactivation, adsorption, inadequate recovery of virus, or physical entrapment of virus particles between the powder particles.

At the end of 24 hours, the performance of S-Cu and UnV-Cu against HCoV was comparable to that of Cu_2O. However, the same powders reduced the titer of PPV much faster relative to Cu_2O. Results of the study suggest that Cu^{2+} infused sepiolite and unexfoliated vermiculite may be just as effective as Cu_2O in reducing viral loads. The relative efficacy can be quantitatively compared by determining the constant rate at which virus is removed by each of the powders.

A quantitative relationship was established between time and removal of virus by fitting 1st and 2nd order kinetic models to the linearized viral titer data obtained for HCoV at different time points. In a chemical reaction, for a first order model, the rate of the reaction depends only on the concentration of the reactant [115]. Analogously, here, the rate of virus removal will depend on the concentration of the virus as described in equation 4.1. For a second order model, the rate depends on the concentration of a single reactant raised to the second exponent or the concentrations of two individual reactants. Since the kinetics of a single virus is considered at a time, the 2nd order model will depend on the concentration of the virus raised to the 2nd exponent as described by equation 4.2.

$$r = \frac{dN}{dt} = k * N \qquad (4.1)$$

$$r = \frac{dN}{dt} = k * N^2 \qquad (4.2)$$

N represents the virus concentration in $\log_{10}$ MTT$_{50}$/mL, *t* is the time in hours and *k* is the first order rate constant in s^{-1}. Final linear models (equations 4.4 and 4.6) to be plotted to obtain the rate constant are derived below:
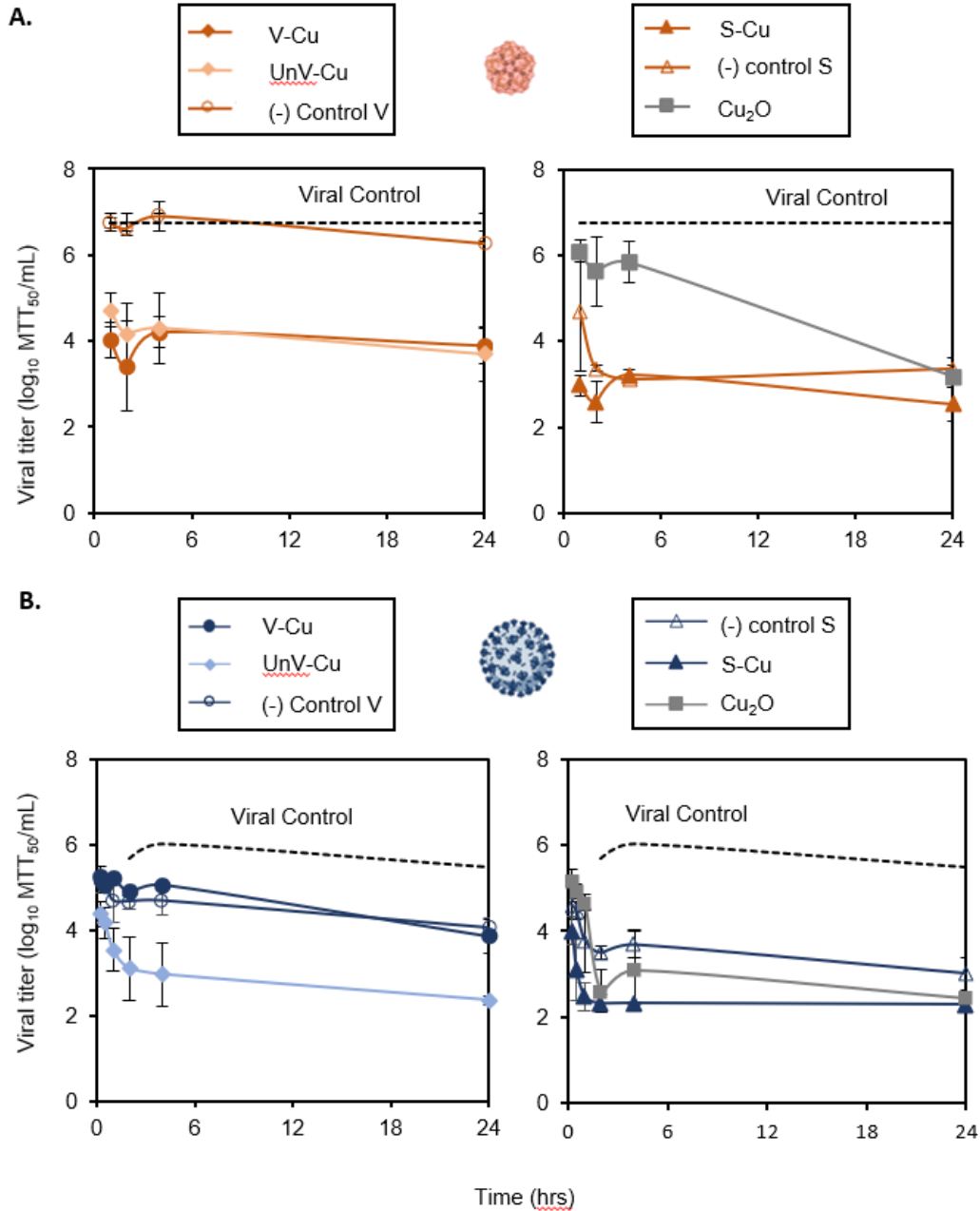
Figure 4.2: Inactivation kinetics A*. kinetics of inactivation observed after treatment PPV with control and Cu^{2+} containing clay mineral powders and Cu$_2$O for 1, 2, 4 and 24 hrs* B. kinetics of inactivation observed for HCoV for treatment times of 15 min, 30 min, 1, 2, 4 and 24 hours. The dashed black line represents the viral control for each of the respective viruses obtained by treating the virus to the same temperature and missing conditions during incubation but in the absence of any clay mineral powder.

Derivation of a first order model for rate of virus inactivation:

The rate of the reaction (r) depends on the concentration of virus (N) raised to the exponent 1 as described earlier by equation 4.1:

$$r = \frac{dN}{dt} = k * N \qquad (4.1)$$

Integration yields

$$\mathrm{Ln}(N) = k * t + C_1 \qquad (4.3)$$

where C_1 is the integration constant

Converting natural log (Ln) to Log base 10 (Log_{10}) since the viral titers obtained using the MTT assay are in units of $\log_{10}$

$$2.3 * \mathrm{Log}_{10}(N) = k * t + C_1 \qquad (4.4)$$

Solving for the integration constant using the initial boundary condition, where at t_0, the initial time point, N_0 is the initial concentration of the virus solution:

$$@t = t_0, N = N_0$$

$$C_1 = 2.3 * \mathrm{Log}_{10}(N_0)$$

Substituting C_1 into equation 4.4:

$$2.3 * \mathrm{Log}_{10}\left(\frac{N}{N_0}\right) = k * t \qquad (4.5)$$

where the slope of graph obtained by plotting $2.3 * \mathrm{Log}_{10}\left(\frac{N}{N_0}\right)$ on the y-axis and t on the x-axis gives the rate constant k.

Derivation of a second order model for rate of virus inactivation:

The rate of the reaction depends on the concentration of virus raised to the exponent 2 as described by equation 4.2:

$$r = \frac{dN}{dt} = k * N^2 \qquad (4.2)$$

$$\frac{1}{N^2} dN = k * dt \qquad (4.6)$$

32

Integrating

$$-\frac{1}{N} = k * t + C_2 \qquad\qquad (4.7)$$

Solving for the integration constant C_2 using the initial boundary condition described earlier:

$$@t = t_0, N = N_0$$

$$C_2 = -\frac{1}{N_0}$$

Substituting C_2 into equation 4.7:

$$\frac{N - N_0}{N * N_0} = k * t \qquad\qquad (4.8)$$

where the slope of the graph obtained by plotting equation 4.8 gives the rate constant k.

Majority of the Cu^{2+} containing powders required up to 2 hours to obtain near maximum reduction in viral titers. Therefore, models for Cu^{2+} containing clay mineral powders were fit to results obtained for incubation time-points of up to 2 hours. V-Cu continued to show inactivation beyond 2 hours, therefore, neither the 1st nor the 2nd order models provided a good fit for the linearized data ($R^2 < 0.75$) over the 2-hour incubation period as shown in figure 4.3 and 4.4. For S-Cu, since a saturation point for HCoV inactivation was obtained following 1-hr of incubation, the 1st order model provided a relatively poor fit ($R^2 = 0.71$) as seen in figure 4.3. Refitting V-Cu 1st order and 2nd order data using time points of up to 24 hours improved the relative fit of the models with R^2 values corresponding to 0.95 and 0.98 respectively (table 4.2). Similarly, refitting the S-Cu 1st order data to time points of up to 1 hr only increased the R^2 value to 0.92 and hence provided a better fit (table 4.2). For the remaining powders, the 1st and 2nd order models provided relatively good fits for the 2-hr incubation data. S-Cu showed the highest observed inactivation rate constant, k for HCoV followed by Cu_2O and then UnV-Cu. Inactivation by V-Cu was the slowest.
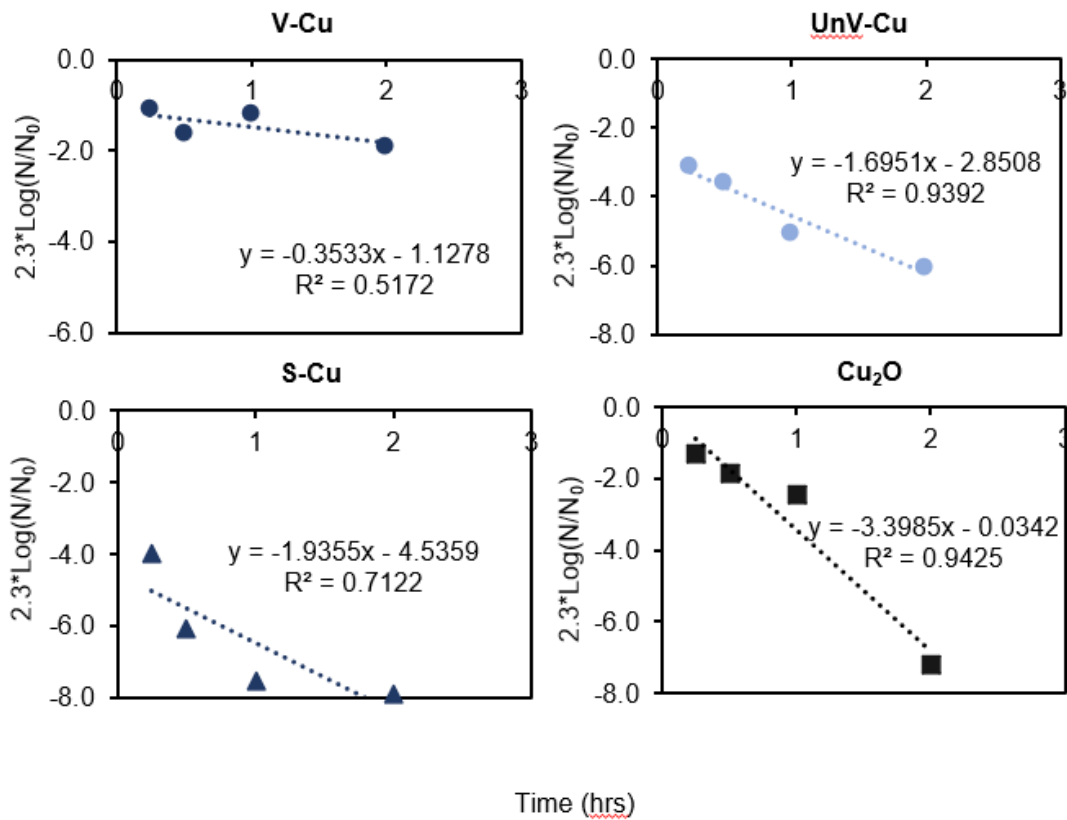
Figure 4.3: Linearized kinetic data to fit a 1st order rate model
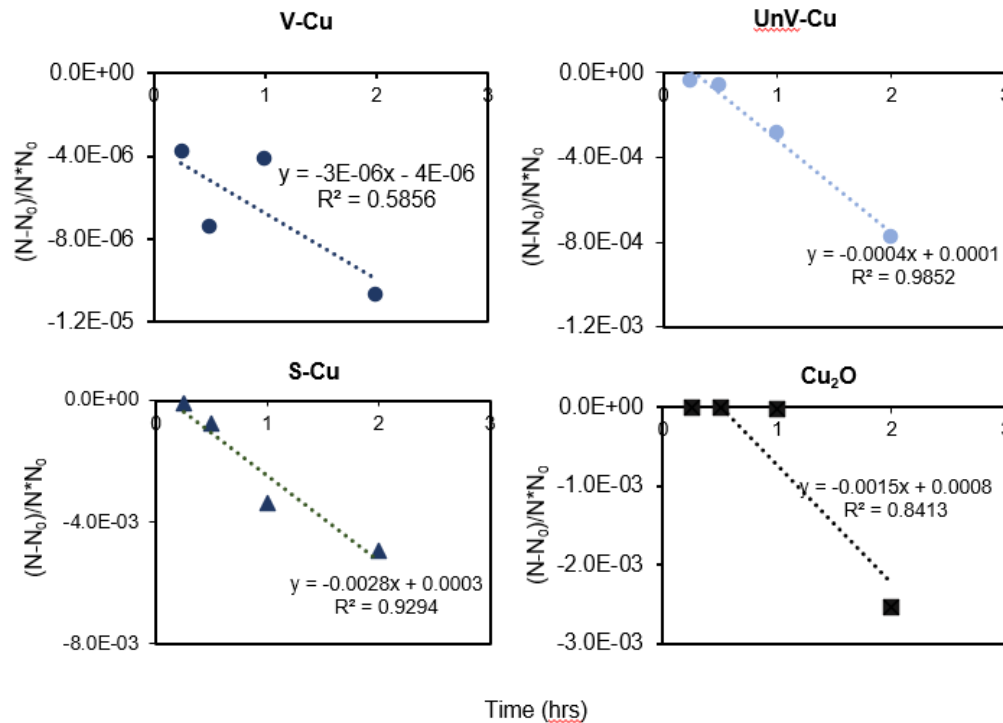
Figure 4.4: Linearized kinetic data to fit a 2nd order rate model

The relative kinetic rate constant of PPV and HCoV removal obtained for each powder are shown in figure 4.5 A and B and tabulated in Table 4.2. The results are in agreement with the inactivation observed. The error on the k values obtained was considerably high (standard deviation not shown). This was to be expected since errors on infectivity assays can be considerably high themselves.
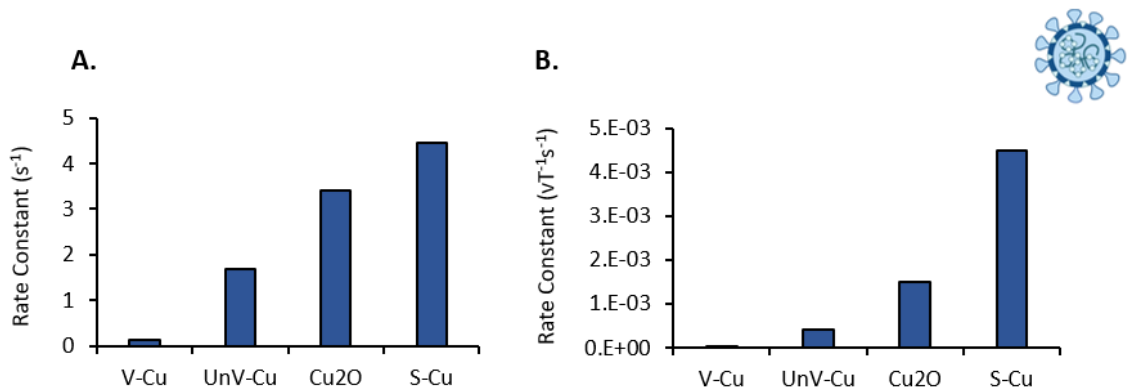
Figure 4.5: Rate constants for HCoV inactivation (graphed for the best fit model depending on time of incubation from table 4.2). A. First order rate constants are in the units of per time (s-1) and B. second order rate constants are in the units of $VT^{-1}s^{-1}$ where VT stands for viral titer in units of $\log_{10}MTT_{50}/mL$.

Table 4.2: Comparison of inactivation rate constants of powders determined for first and second order of inactivation kinetics.

Sample	Virus	Time (hrs)	1st order k (s^{-1})	1st order R^2	2nd order k ($VT^{-1}s^{-1}$)	2nd order R^2
Cu_2O (+ve Control)	PPV	24	0.28	0.98	3.00E-05	0.99
Cu_2O (+ve Control)	HCoV 229E	2	3.40	0.94	1.50E-03	0.84
UnV-Cu	HCoV 229E	2	1.70	0.94	4.00E-04	0.99
V-Cu	HCoV 229E	2	0.35	0.52	3.00E-06	0.59
		24	0.13	0.95	6.00E-06	0.98
S-Cu	HCoV 229E	2	1.94	0.71	2.80E-03	0.93
		1	4.46	0.92	4.5E-03	0.98

4.1.4 Cytotoxicity of clay mineral powders

In addition to antiviral testing, the powders were evaluated for potential cytotoxic effects against the indicator cell lines PK-13 and MRC-5 used for PPV and HCoV, respectively. A suspension of the clay mineral powders was prepared in HEPES buffer and incubated for 24 hours as previously described for the antiviral studies. Following incubation, the suspension was centrifuged, and the supernatant was retrieved to check for cytotoxicity. The supernatant (25 µL) was directly added to the first column of wells of a 96-well plate containing a monolayer of the indicator cells and serially diluted at a 1:5 dilution. The results are shown in figure 4.6.

PK-13 cells used as the indicator cell line for measuring PPV infectivity showed a near 25% drop in the percent viability of the cells following propagation with the highest concentration of the Cu^{2+} containing vermiculite powders, V-Cu and UnV-Cu, possible following incubation (figure 4.6A). Despite the drop, the percent cell viability was maintained over 70% and should not affect the viral titers reported as the MTT assay determines values based on a 50% cell viability [100]. Similar results were obtained with the sepiolite control and Cu^{2+} infused powder, S and S-Cu. The positive control, Cu_2O also maintained PK-13 cell viability over 70%. For MRC5 cells, V-Cu and UnV-Cu reduced the cell viability by 23% and 17% respectively, while maintaining average cell density over 70% (figure 4.6B). S-Cu also reduced cell viability to 70%. The largest drop was observed with Cu_2O (~44%) which was increased to over 70% following a five-fold dilution. It is difficult to make a definite conclusion regarding the cytotoxicity of the powders towards the indicator cell lines utilized. However, for the purpose of this study,

the powders did not interfere with the ability of the MTT assay to evaluate virus infectivity.
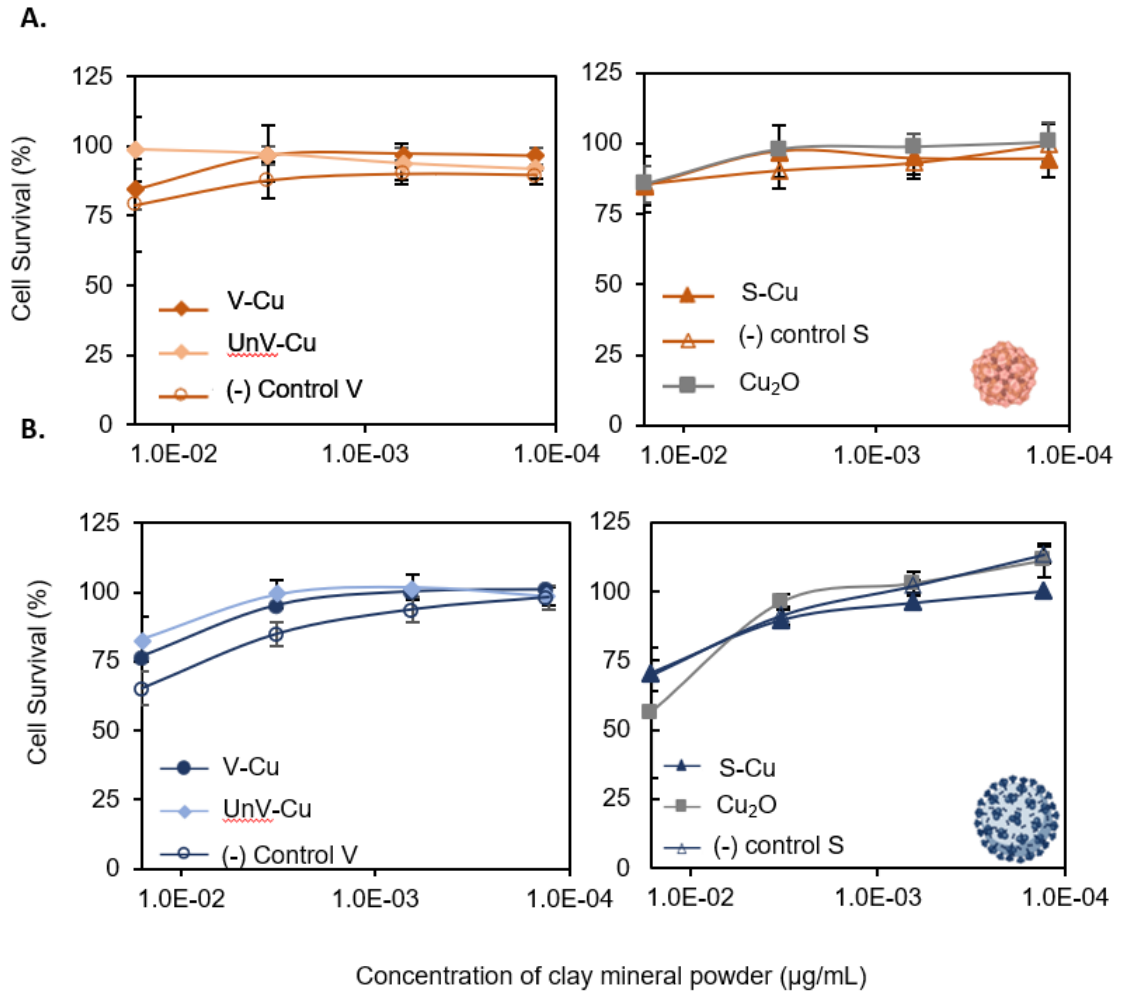
Figure 4.6: Evaluation of cytotoxicity of copper infused clay mineral powders against **A*.** PPV and **B.** HCoV.

* Data obtained by Vaishali Sharma

4.1.5 Mechanism of virus removal

The ability of Cu^{2+} containing novel powders to reduce virus titers in a time-dependent manner was demonstrated. However, the results provided no confirmation regarding the mechanism of inactivation. For vermiculite powders, the results indicated Cu^{2+} directly contributed towards virus inactivation. However, with sepiolite, the activity of Cu^{2+} ions were unclear due to the high adsorptive property of the clay mineral.

Moreover, each Cu^{2+} containing powder reduced the viral burden to different extents depending on the powder and the virus.

An initial hypothesis was developed to obtain insight into the mechanism of inactivation. We believed addition of virus solution to suspensions of clay mineral released Cu^{2+} ions into the solution [98]. As a result, the solution based Cu^{2+} would interact with the virus to generate ROS and degrade the viral genome or viral proteins [51, 127]. The total amount of Cu^{2+} released into solution was obtained using inductively coupled plasma mass spectrometry (ICP-MS). To confirm the role of Cu^{2+} in virus removal, EDTA, a common agent to chelate metal-ions used. Hypothetically, EDTA should chelate any released Cu^{2+} and render the powders ineffective as antiviral materials [128].

Quantification of Cu^{2+} release

Release of Cu^{2+} was quantitated with ICP-MS. Three different buffers, HEPES (0.025 M), PBS (1X, pH 7.2) and distilled water were used with results reported in table 4.3, 7.1 and 7.2 respectively. Each control and copper containing powder (0.02 g) was treated with 1 mL of each of the buffer solutions in a 360° rotation motion for 2 hours at 4 °C. The 2-hour time point was chosen as a considerable reduction in viral titer was observed after 2 hours in the kinetics study. Table 4.3 compares the amount of metal ions released by the Cu^{2+} containing powders with their respective controls. Successful displacement of Mg^{2+} was observed, comparing unmodified V and S with Cu^{2+} containing specimens. However, the amount of Cu^{2+} leached was not proportional to the amount of Mg^{2+} ions displaced. In fact, very little Cu^{2+} was leached using the three buffers in a time independent manner (results for PBS, DI water and 24-hour incubation can be found in appendix 7.2. Maximum leaching occurred with 25 mM HEPES in 2 hrs. Release of Cu^{2+} in ppm was reported in the order of UnV-Cu (5 ppm) > S-Cu (0.267 ppm) > Cu_2O (0.066 ppm) > V-Cu (<0.05 ppm) as shown in table 4.3. Relatively higher amounts of Cu^{2+} may have been leached from UnV-Cu potentially due to the higher distribution of Cu^{2+} on the surface of the powder. The same ions may be present within the deep layer of exfoliated counterpart. Very low concentrations of Cu^{2+} were leached from Cu_2O which is in agreement with the poor solubility exhibited by several metal oxides in water [129]. Overall, a low release of Cu^{2+} was observed and the data was not conclusive enough to suggest virus inactivation is due to solution-based ions.

Table 4.3: ICP testing of control and copper treated clay mineral powder with 0.025M HEPES solution for 2 hours showed minimal release of cupric ions in solution (Provided by Dr. Bowen Li)

Sample	Cu (ppm)	Mg (ppm)
UnV-Cu	4.764	0.078
V-Cu	<0.05	60.4
V	<0.05	85.24
S-Cu	0.267	47.07
S	<0.05	20.72
Cu_2O	0.066	61.34

Role of solution based Cu^{2+} in virus removal

The role of solution based Cu^{2+} ions as the potential antiviral agents was further assessed by chelating Cu^{2+} ions released in solution with 1 mM EDTA. Three different cases were considered. In case 1, EDTA was added to the virus-clay powder suspension prior to incubation (pre-EDTA). In case 2, EDTA was added to the virus-clay suspension after incubation (post-EDTA). Lastly, in case 3, no EDTA was added (no-EDTA). The studies were performed only with the non-enveloped virus model, PPV. If solution based Cu^{2+} ions were involved in inactivation, the viral titers for the post-EDTA and no-EDTA cases should be comparable. In the pre-EDTA case, no reduction of virus titer should be observed as EDTA added prior to treatment should chelate any Cu^{2+} ions released over the course of the incubation period. The results for the three cases tested are shown in Figure 4.7. No comparable difference was observed between the pre-EDTA and No-EDTA cases for Cu^{2+} infused sepiolite (p value > 0.05). However, some chelation of Cu^{2+} was observed for both UnV-Cu and V-Cu in the pre-EDTA and post-EDTA case. This chelation for UnV-Cu may be a result of the ~5ppm release of Cu^{2+} ions observed in the ICP-MS testing. However, the same cannot be concluded about V-Cu since < 0.05ppm of Cu^{2+} ions were leached into solution by the V-Cu powder. These results provide no conclusive evidence to support the initial hypothesis for virus inactivation by solution based Cu^{2+} ions for V-Cu and S-Cu. Addition of EDTA prior to treatment should have chelated all or majority of the Cu^{2+} present in solution, rendering them ineffective as antiviral agents. This seemed true for UnV-Cu but not for the remaining powders including the positive control powder Cu_2O.

Neither the ICP nor EDTA study provided conclusive results to confirm if Cu^{2+} ions were leached into solution and that they participated in virus removal or inactivation. However, lack of reconciliation between the amount of Mg^{2+} ions displaced vs. Cu^{2+} in the ICP data suggests the inability to leach all the ions into solution. Additionally,

chelation of solution based Cu^{2+} had little impact on the ability of the powders to reduce viral titer. These findings allude to a surface adsorption-based contact-killing mechanism as previously reported [93].
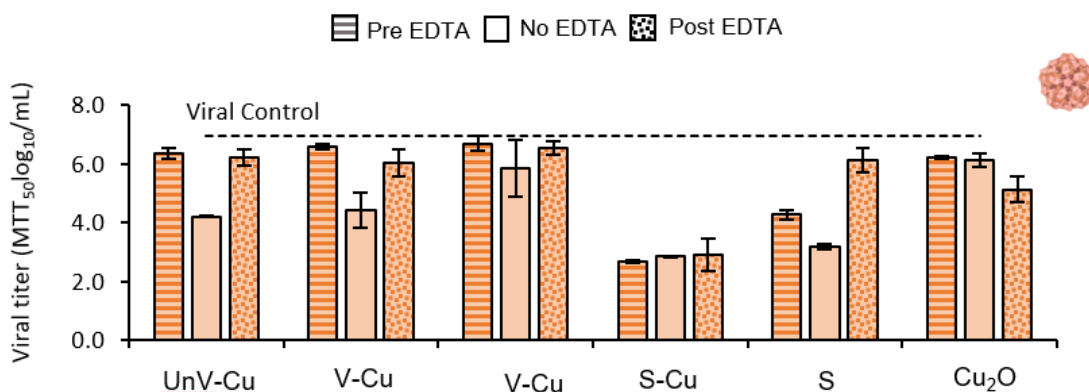
Figure 4.7: Viral titers observed for PPV (i)Pre-EDTA, addition of 1 mM EDTA to virus-clay suspension prior to incubation (ii) No EDTA, no EDTA added, 25 mM HEPES was added to maintain sample volume and (iii) Post-EDTA, addition of 1 mM EDTA to virus clay suspension after incubation for 2 hrs at 4 °C in 360° rotation motion.

*Data collected by Vaishal Sharma

Role of surface incorporated Cu^{2+} ions in virus removal

Inability of solution-based ions to reduce virus titers was demonstrated. In fact, as per ICP-MS data, majority of the ions remained incorporated into the powders. An alternative surface attachment-based mechanism for virus removal and inactivation was hypothesized. Bovine serum albumin (BSA), a known blocking agent was added to block Cu^{2+} sites present on the surface of the clay mineral powders. Addition of BSA to the virus clay suspensions of both PPV and HCoV prior to incubation inhibited the antiviral effect of the powders as seen in figure 4.8. Without BSA, the Cu^{2+} infused clay powders reduced the titer of PPV (figure 4.8 A) and HCoV (figure 4.8 B). However, with BSA, no virucidal activity was observed. The difference was more remarkable for the non-enveloped virus model as the vermiculite samples reduced PPV titers to a greater extent due to its relatively smaller size as discussed before. The data with BSA provided confirmation towards a contact based, adsorption mechanism of virus inactivation by the integrated Cu^{2+} ions.
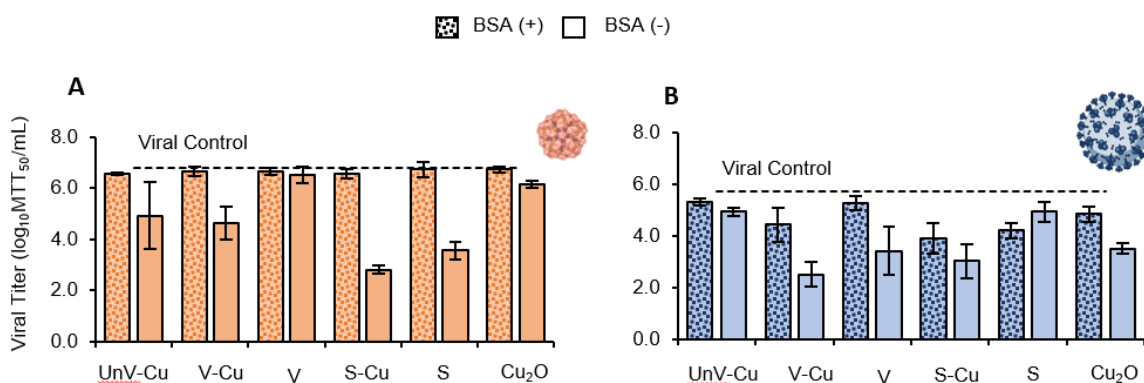
Figure 4.8: Viral titers observed for A. PPV* and B. HCoV 229E (right) after incubation with and without 1% BSA for 2 hrs at 4 °C in 360° rotation motion.

*Data collected by Vaishali Sharma

Phyllosilicate minerals, vermiculite and sepiolite, were successfully infused with Cu^{2+} and imparted antiviral properties to the clay minerals. The degree of inactivation of the two model viruses was proportional to contact time between the Cu^{2+} infused powders and viruses. However, the mechanism and extent of inactivation or virus removal varied between the powders and the viruses studied. The difference observed between V-Cu and UnV-Cu was attributed to the relatively smaller size of PPV. We hypothesize exfoliation of the vermiculite samples caused Cu^{2+} to be in the deep layers hard to access for HCoV. However, PPV being relatively smaller (~20 nm), experienced little restriction to accessing Cu^{2+} rich sites in the exfoliated powder. Comparison of results between the control vermiculite powders with their Cu^{2+} infused powders for both HCoV and PPV, suggested that the reduction in viral titers was due to inactivation activity of Cu^{2+} alone and not insufficient virus recovery from the test samples. However, a combinatory effect of the adsorptive (for virus removal) and Cu^{2+} integration (for virus inactivation) of the sepiolite powder was observed in reducing the titers of PPV and HCoV.

The final hypothesis towards virus inactivation by Cu^{2+} containing ions alludes to a surface-based mechanism of inactivation (figure 4.9) as the amount of copper leached by the buffers was found to be insufficient to observe significant inactivation. Inactivation by exfoliated vermiculite containing Cu^{2+} followed first order kinetics of inactivation over 24 hrs. The remaining copper infused clay powders – unexfoliated vermiculite, sepiolite and the positive control Cu_2O, all followed second order kinetics over the first 2 hrs of treatment. Maximum inactivation was observed by sepiolite in as little as two hours. The study presented significant inactivation, considering, the experimental conditions were set for a worst-case scenario.
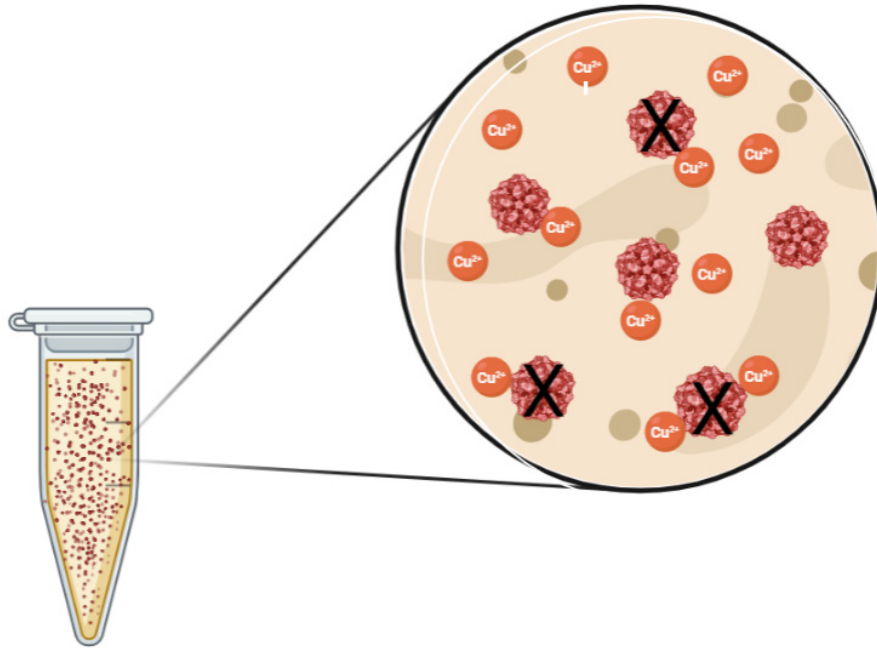
Figure 4.9: Surface attachment of virus (PPV) and interaction with interlayer cupric ions for virus inactivation. Figure created in biorender.com.

Most antiviral studies with clay minerals assume very low ppm concentrations of copper in the lixiviate to be sufficient to inactivate virus without accounting for the remaining amount of metal ions/ nanoparticles present in the clay mineral. There is a gap in literature demonstrating the efficacy of surface incorporated metal ions/ nanoparticles against viruses. We propose the high sportive capacity of clay minerals along with van der waals and hydrophobic interaction of the clay mineral with virus particles to be responsible for virus inactivation. Moreover, studies with BSA, the blocking agent that inhibits non-specific binding, showed that presence of BSA significantly reduced inactivation.

The study has potential for further research and optimizations. Inactivation kinetics at a different temperature, treatment of lixiviates from copper containing powders with virus solution, different concentration of powders (wt%), pH etc can be studied as well. However, for our recommended application of fillers for paint for high frequency touch surfaces, the results of the inactivation studies demonstrate the ability of copper treated powders to adsorb and either inactivate or remove virus particles. This is rather relevant to the current ongoing pandemic with the highly infectious SARs CoV-2 virus and any future occurrences with a new outbreak to restrict and mitigate disease transmission.

4.2 C_{12}-benzophenone functionalized melt-blown and spun-bound polypropylene fabrics

Inhalation of pathogen-rich, airborne aerosols or liquid droplets are the leading cause of direct, contact-based transmission of diseases. Yearly, highly pathogenic, and transmissible respiratory viruses such as influenza virus, rhinovirus and coronavirus infect people worldwide [5, 6]. Physical barriers like personal protective equipment (PPE), particularly facial coverings, are reported as effective engineering tools in mitigating the spread of respiratory illnesses. Following the COVID-19 pandemic, numerous studies demonstrated the efficacy of surgical and N95 masks in reducing the burden of infection [48]. N95 masks are able to filter 95% of pathogen particulates less than 0.3 microns in size [49]. Moreover, complaint use of masks considerably lowered the risk of influenza and other respiratory viruses [117, 118].

Filtration efficiency, appropriate fit and comfort (breathability) are key design considerations in improving the quality of face masks. Particles emitted by an infected individual can range from 0.01 micron to more than 1 mm in size. Filtration efficiency of a fabric depends directly on the particle size. Normally, most masks, even cloth masks are able to effectively filter particles greater than 10 microns in size. However, this size is far too large for the pathogens potentially inhabiting droplets less than 10 microns in size. Different fabrics made of woven, non-woven (polypropylene and cellulose) or knit materials can be layered intricately with a tight control over the pore size, to generate masks with high filtration efficiency and breathability [119].

Recent developments in the design considerations of face coverings include physical or chemical modification of the layers of the WHO approved 3-layer format for N95 masks or single-ply surgical masks. A standard 3-ply mask consists of an inner layer to absorb moisture, a middle melt-blown layer to filter particulates, and an external hydrophobic layer to limit droplet deposition and entry [61]. Surface roughening, a physical modification to the outermost layer of the mask, aims to improve surface hydrophobicity to reduce accumulation of pathogenic load. Chemical modifications through functionalization of biocidal agents like silver ions and silicon dioxide aim to inactivate virus upon contact [62]. However, the listed methods suffer limitations. Physical modifications, while prevent infection, do little to control the viral load of the immediate surrounding. Chemical modifications provide the benefit of virus inactivation but suffer from limitations of duration of efficacy and stability.

This study proposes the functionalization of non-woven, spun-bound and melt-blown, polypropylene masks with an antiviral agent, C_{12} quaternary ammonium benzophenone. Quaternary ammonium compounds (QACs) belong to a class of cationic biocides and are frequently used domestically and commercially to meet daily disinfection needs. QACs, like cupric ions in the previous study, are known to inactivate a broad spectrum of viruses [74]. The antiviral effect of QACs is attributed to their ability to disrupt phospholipids. The alkyl chains of the cationic compounds can permeate the membrane, while the positively charged nitrogen atom can remain within the surface of the membrane. As a result, the virus can undergo severe changes in its physical and

biochemical properties and the surface charge distribution [56]. The application of antiviral QACs in PPE can be extremely beneficial to mitigating disease spread.

Two grafting methods via covalent linking and physisorption of the QA salts were explored with both melt-blown polypropylene (mbPP) which constitutes the filtration layer in a standard 3-ply N95 mask, and spun bound polypropylene (sbPP), often used in surgical masks or as the outermost layer in N95 masks. The antiviral efficacy of each modified non-woven fabric was tested with the enveloped suid herpesvirus (SuHV-1) and human coronavirus (HCoV 229E).

4.2.1 Functionalization of mbPP and sbPP with QA compounds

Two C_{12} quaternary ammonium compounds N-(4-Benzoylbenzyl)- N,N-dimethyldodecan-1-aminium bromide (QA1) and Poly(1-dodecyl-4-vinyl pyridinium bromide) (QA2) were prepared with slight modifications to methods described in literature [120, 121]. Two polypropylene based non-woven fabrics, melt-blown PP and spun-bound PP, used as filtration media in masks, were modified with synthesized compounds QA1 and QA2 [102]. Compound QA1 was covalently grafted on to the two fabrics while, compound QA2 was physiosorbed to the filtration media as described in figure 4.10A and B. UV light at 254 nm was used in the polymerization and grafting process to facilitate formation of ultra-thin polymer coatings with a permanent cationic charge (figure 4.10C). This step was crucial to the grafting process to impart long-term antiviral properties to the filtration media.

4.2.2 Zeta potential, filtration efficiency and pressure drop

Zeta potential measurements confirmed successful grafting of the two QA polymers onto the filtration media. Zeta potential of uncoated melt-blown PP and spun-bound PP were measured as -58.5 mV and -63.8 mV respectively, both values consistent with previous publications [102]. Covalently grafted QA1 melt-blown PP sample showed zeta potential of 47.1 mV, and thus complete reversal of charge distribution (figure 4.10D). Physiosorbed QA2 melt-blown PP sample had zeta potential of -4.2 mV, which represents higher cation charge distribution than the uncoated melt-blown PP, but drastically fell short in comparison to the QA1 grafted polymer coating. Zeta potential of the QA grafted spun-bound PP filters were relatively lower. Moreover, treatment with ethanol further reduced the zeta potential of QA1 grafted spun-bound PP suggesting incomplete covalent grafting of the polymer to the fabric.

After the incorporation of the QA compounds, the filtration efficiency (FE) and pressure drop (PD) across the filter media were characterized per the standards established by NIOSH for certifying N95 masks. A full uncoated N95 mask showed filtration efficiency of 92.4%. However, the FE of single-ply QA1 and QA2 coated melt-blown PP dropped drastically to 51.3% +/- 7.8% and 54.2% +/- 0.3% respectively as shown in figure 7.1. Exposure to organic solvents like isopropanol and acetone used in the coating process may have contributed to this loss in FE. While FE suffered, the modified fabrics-maintained PD, thereby having no impact on breathability. FE and PE were also measured for a N95 prototype sandwiching two QA coated melt-blown PP

layers between the QA1 grafted spun-bound PP. Such an arrangement allowed recovery of FE to 99.7% without negatively impacting PD [102].
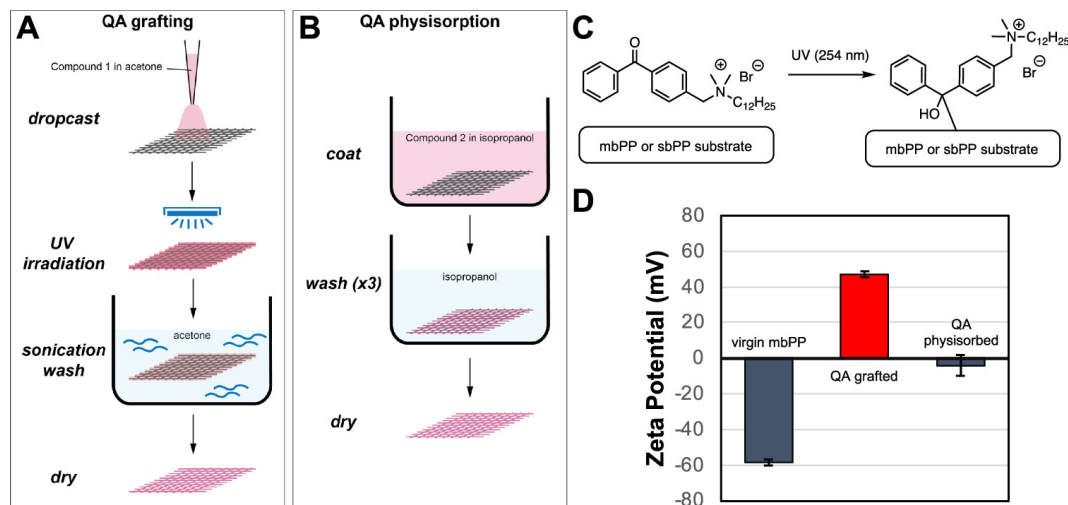
Figure 4.10: Covalent grafting (A) and physisorption (B) of QA1 and QA2 compounds, respectively, onto filtration media at UV light 254 nm (C) followed by zeta potential measurements (D), Figure and data provided by collaborators from RPI [102]. Figure reprinted from reference # 102, Copyright 2022, Sorci et. al., published under license CC BY-NC-ND 4.0.

4.2.3 Antiviral effect of QA functionalized mbPP and sbPP

The virucidal activity of QA-coated filters was assessed using the colorimetric MTT assay for infectivity which quantitatively measures host cell metabolic activity [100]. Two enveloped viruses, SuHV-1, and HCoV 229E, a model for respiratory viruses were used in the study. The MTT_{50} infectivity assay yields viral titer results in units of $\log_{10} MTT_{50}/mL$. However, in our case, the working volumes for the wash and the elution step were different. Therefore, the final values were, instead reported in units of $\log_{10} MTT_{50}$. The log reduction value was determined by subtracting the viral titers observed for each sample from the viral control. All experiments were performed in triplicates to ensure consistency in the result.

QA1-grafted melt-blown PP filters showed 3.7 and 3.3-log reduction in viral titer for the wash and elution steps, respectively for SuHV-1 (Figure 4.11A). Here, a high LRV (described by equation 3.1) for the wash step indicates a low virus titer, suggesting that majority of the virus particles were able to bind with the filters as projected. No virucidal activity was observed against SuHV-1 with bare and QA2 physisorbed melt-blown PP.

For HCoV, 2.2 and 2.3-$\log_{10}$ reduction were observed for the QA1-grafted melt-blown PP in the wash and elution steps respectively (Figure 4.11B). However, high LRVs were also observed with bare melt-blown PP and physisorbed QA2 filters even in the

wash step. These high LRVs suggest the inability to completely elute HCoV from the filters. This non-specific binding has been reported as a common occurrence with certain enveloped viruses in literature [122], making it difficult to assess the antiviral activity of the coated filters against HCoV. Interestingly, no antiviral activity was observed with the grafted and physisorbed spun-bound PP filters for both SuHV-1 and HCoV. This finding is consistent with the low reversal of surface charge density observed in the zeta potential results for QA1 grafted and QA2 physisorbed spun-bound PP filters. Overall, this demonstrated that the functionalization of the QA polymer was less successful on the spun-bound PP filter in comparison to the melt-blown PP filter.
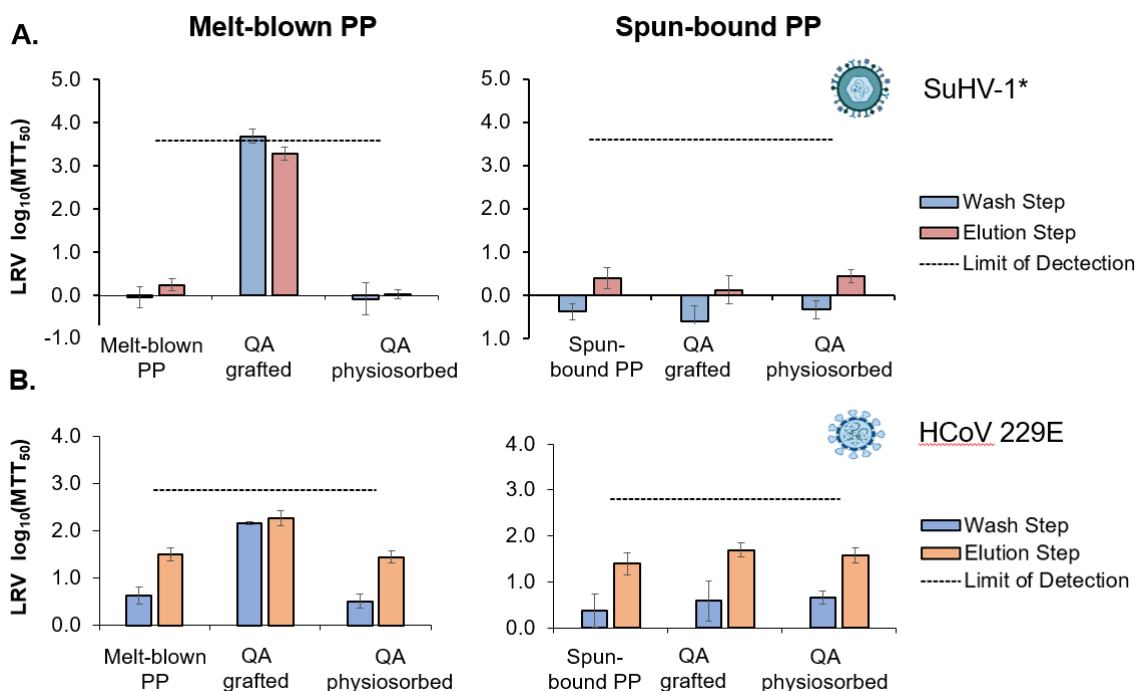
Figure 4.11: Antiviral efficacy of QA1 grafted and QA2 physisorbed melt-blown PP and spun-bound PP against A.* SuHV-1 and B. HCoV-229E. Results are reported in LRV. The wash step with phosphate buffer following incubation removed any unbound virus and the elution step facilitated complete recovery of virus from the fabric post incubation. Figure reprinted from reference # 102, Copyright 2022, Sorci et. al., published under license CC BY-NC-ND 4.0.

*Data collected by Sneha Singh and Vaishali Sharma

Adequate wetting of the QA grafted and physisorbed fabrics was crucial to virus attachment and inactivation. The wetting procedure described previously was effective in wetting QA1 grafted and QA2 physisorbed melt-blown PP but not the modified, more hydrophobic, spun-bound PP non-woven filters. This finding is consistent with the

physico-chemical properties of the two non-woven fabrics. No bonds form between the filaments of the extruded molten fabric during the production process of melt-blown PP fabrics. However, in the case of spun-bound PP fabrics, weak bonds are formed [59, 60]. As a result, spun-bound PP fabric tends to be much softer, less porous, stronger and more durable. Covalently grafted QA1 with highest cationic charge distribution was most effective in reducing viral titers. Virus attachment facilitated the antiviral action of the cationic quaternary ammonium salt. A proposed mechanism for virus inactivation is shown in figure 4.12. High LRVs were observed with enveloped viruses, SuHV-1 and HCoV. Physiosorbed QA2 melt-blown PP was not as effective, consistent with the relatively lower positive charge density observed on its surface.
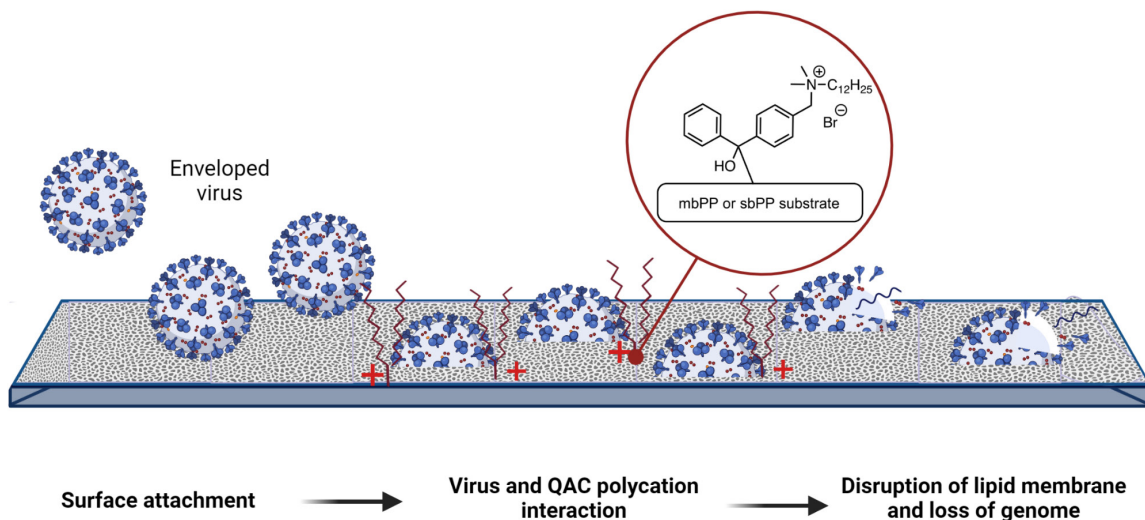
Figure 4.12: Proposed mechanism for virus inactivation. The aliphatic chain of QAC disrupts the viral lipid envelope, allowing the positively charged nitrogen from the amine functional group to disrupt viral proteins and facilitate the loss of viral genome; created in biorender.com.

In summary, C_{12} quaternary benzophenone were successfully incorporated as ultra-thin coatings for mbPP, used as the filtration layer of N95 masks and sbPP, used in surgical masks. QA1 covalent grafting resulted in maximum reversal of positive charge density on the surface of the fabric. However, it lowered filter efficiency from 70% down to 50%. The QA1 modified mbPP was also most effective in inactivating enveloped viruses SuHV-1 and HCoV. Adequate wetting of fabric was crucial to virus attachment and inactivation. The QA grafted sbPP fabrics were relatively more hydrophobic, making virus attachment difficult. They also showed low cationic surface charge distribution but higher filtration efficiency. The modified sbPP layer, while, not effective as a potential antiviral agent, could be used as the outermost layer of N95 masks to resolve/compensate for the low filtration efficiency of the QA1 covalently grafted mbPP filter.

4.3 Catechol coated melt-blown polypropylene fabrics

Respiratory droplets emitted by an infected individual are the leading cause of widespread respiratory illnesses. SARs CoV-2, a highly infectious respiratory virus, caused the COVID-19 pandemic and resulted in over 6 million deaths worldwide. While common chemical and physical tools for disinfection like isopropyl alcohol, sodium hypochlorite, UV and heat show promising results for virus inactivation, they are either too harsh or require external stimuli for activation. The persistence of airborne viruses on surfaces poses an additional challenge to manage disease transmission. This study proposes the development of a self-sanitizing coating on non-woven melt-blown polypropylene (mbPP) based facial coverings through catechol polymerization. A catechol-based coating with 6-hydroxydopamine is developed which releases hydrogen peroxide, a known antiviral agent, upon contact with the moisture in respiratory droplet.

This is a biomimetic application inspired by marine mussels. Marine mussels incorporate a series of post-translationally modified amino acids such as L-3,4-dihyroxyphelylalanine (DOPA) to overcome adhesion challenges underwater. Interfacial bonds are formed between DOPA rich, secreted proteins (~20 mol%) to facilitate adhesion [123]. During the adhesion process, the catechol functional group of DOPA undergoes oxidation to form quinone, the sticky moieties and release H_2O_2 as a byproduct. This study exploits this mechanism to facilitate release of H_2O_2 using 6-hydroxydopamine.

Hydrogen peroxide, known for its antimicrobial properties, is commonly used as a disinfectant to inactivate a broad spectrum of viruses. A study using a 3% solution of hydrogen peroxide showed 6-log reduction in viral titers of both RNA and DNA viruses in 2 hours [124]. As a strong oxidizing agent, H_2O_2 is believed to irreversibly damage viral proteins, genome or the bilayer, through the release of toxic hydroxyl radicals. Moreover, H_2O_2, degrades into biocompatible products water and hydrogen, neither of which pose particular a hazard to the environment [125].

Compliant use of masks has been highly effective in preventing infection or reducing severity of infection [48, 50]. This study aims to couple the high virucidal activity of hydrogen peroxide with a physical barrier such as facial coverings made of non-woven fabrics to reduce the transmission of highly infectious viruses such as SARs CoV-2. Successful polymerization with the catechol moiety was characterized without significant loss of filtration efficiency. The virucidal activity of the polymers through H_2O_2 release was quantified in a time dependent manner and related to virus inactivation. Polymerization with dopamine methacrylamide, an established platform for virus inactivation through the release of H_2O_2 [125], was used a comparative tool to demonstrate the efficacy of the novel catechol polymer.

4.3.1 Characterization

A catechol containing copolymer, AA-DA-OH-co-AAm, was prepared using AA-NHS, AAm, and 6-OHDA as previously described in figure in 3.4. The final copolymer was characterized using proton nuclear magnetic resonance (^{1}H-NMR) and UV-vis spectroscopy. The final concentration of the 6-OHDA in the copolymer solution was estimated to be 27.8 mol%. A 5 wt% solution of the copolymer in dimethyl sulfoxide was used to coat the bare mbPP fabric. The volume of the solution was adjusted to obtain final coatings of 30 and 40 wt% of the copolymer on the fabrics. The coated samples were imaged using field emission scanning electron microscopy (FE-SEM) to assess sample morphology as shown in figure 4.13. Visual evaluation of the FE-SEM images along with the n-butanol uptake assay revealed that copolymerization did not have a drastic effect on fabric porosity. The porosity was maintained at 80%.
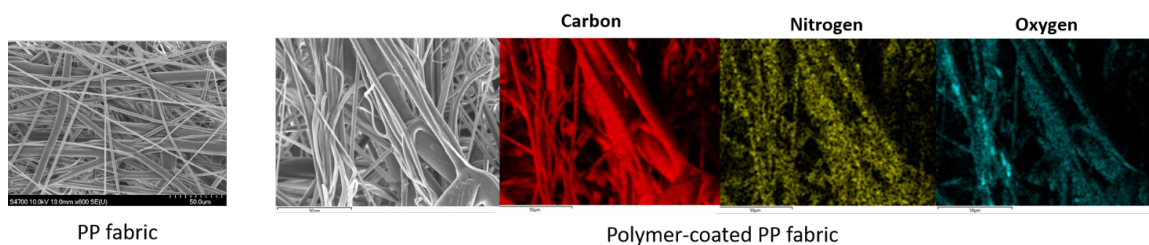
Figure 4.13: FESEM image of PP fabric(left) and fabric coated of catechol containing polymer (right). Copolymer solution prepared, coated and samples imaged by Fatemeh Razaviamri.

4.3.2 Quantitation of hydrogen peroxide release

The ability of the fabric to release hydrogen peroxide (H_2O_2) was evaluated over a 24-hour period using the ferrous oxidation-xylenol orange (FOX) assay. Both the 30 wt% and 40 wt% 6-OHDA based copolymer coatings generated nearly 4mM of H_2O_2 (Figure 4.14) over 24 hours at room temperature. A previous publication with dopamine methacrylamide (DMA) in hydrogels demonstrated H_2O_2 concentrations of 1-5 mM were sufficient to inactivate enveloped viruses [125]. Co-polymerization of the mbPP fabric with DMA in the same quantities as the novel co-polymer yielded a much slower and lower release of H_2O_2 (~1.3 mM) upon hydration. The 6-OHDA based coating generated nearly 3000 more times the quantity of H_2O_2, demonstrating rapid catechol oxidation and H_2O_2 generation and thus superior performance for this particular application.
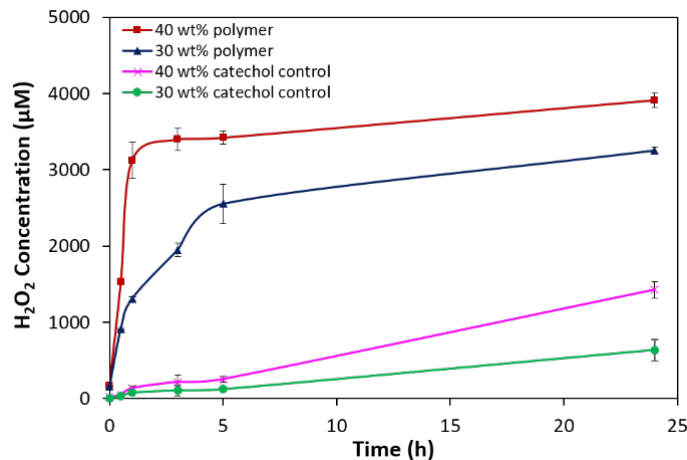
Figure 4.14: H_2O_2 release profile observed for 6-OHDA and DMA copolymer-based coatings upon hydration with 100 µL PBS (1X, pH 7.4). Provided by Fatemeh Razaviamri.

4.3.3 Antiviral activity

The virucidal activity of the 6-OHDA based coatings was evaluated against the enveloped virus model, bovine diarrhea virus (BVDV) and HCoV, a virus model for respiratory viruses. The moisture (H_2O) from the crude virus solution was hypothesized to activate the coating. Oxidation of the catechol groups in the co-polymer generates H_2O_2, the active virucidal agent to inactivate virus as shown in figure 4.15. Since the objective of this study was to demonstrate virus inactivation with H_2O_2 at relatively low concentrations in aqueous solution (upto 4 mM), enveloped viruses, due to the presence of the more fragile lipid bilayer, were chosen as the model viruses. Low concentrations of H_2O_2 (1-3%) have been reported as being effective against enveloped viruses [126]. Higher concentrations of H_2O_2, particularly in aqueous solutions, are required to inactivate the more resistant non-enveloped viruses such as poliovirus [55].

Bare mbPP coated with 30 wt% and 40 wt% 6-OHDA based copolymer solution showed a 2.2 log-reduction in the titer of BVDV after incubation for 24 hours at room temperature (figure 4.16A and B). This corresponds to a 99.4% reduction in the viral load. Moreover, the reduction in viral titer was a function of time, confirming the sustained release of H_2O_2 as previously observed with the fox assay. Bare mbPP and mbPP coated with 30 wt% and 40wt% control coating (NHS and AAm copolymer) lacked the catechol moiety and therefore did not show virucidal activity. The antipathogenic performance of the 6-OHDA based copolymer coating was compared to a DMA based copolymer coating. In a previous study, DMA containing hydrogels inactivated the enveloped BVDV and the non-enveloped virus PPV by the release of hydrogen peroxide at physiological pH 7.4 and temperature 37 °C [125]. Inactivation results observed with the DMA based coating were in agreement with the results observed with the FOX assay. About 1 mM H_2O_2 generation was observed, following hydration after 24 hours. This concentration was too low to show any virucidal effect

against BVDV. No significant difference was observed in the virus titers obtained with the 30 wt% and 40 wt% control coatings and those containing DMA (p value > 0.05).
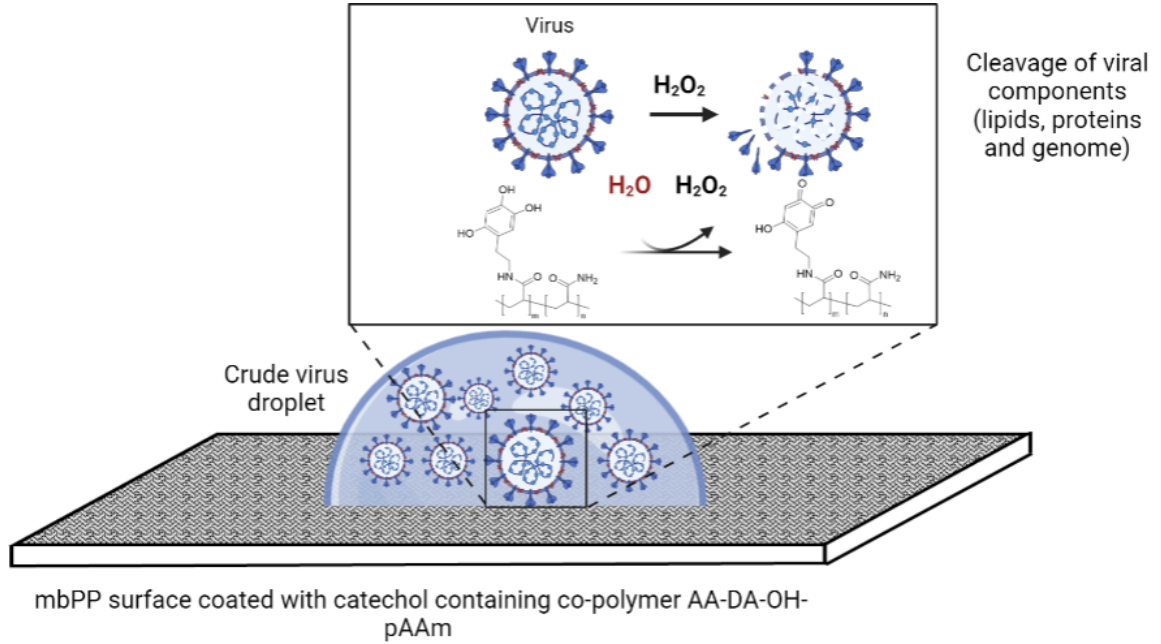
Figure 4.15: Proposed mechanism for inactivation of virus. Water molecules from the crude virus droplet oxidize the catechol groups of the co-polymer to generate H_2O_2. Hydrogen peroxide can cleave or crosslink biomolecules like the viral lipid envelope, capsid proteins and nucleic acids. Figure created in biorender.com.
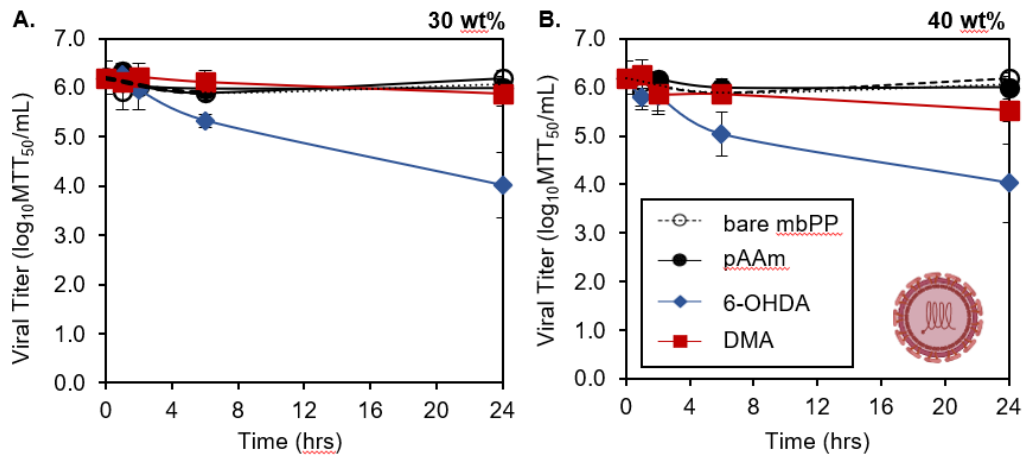
Figure 4.16: Time-dependent inactivation of BVDV. A drop of crude BVDV solution was incubated with bare and coated non-woven mbPP for 0,1, 2, 6 and 24 hours at room

temperature to provide A. inactivation kinetics for 30wt% coatings and B. 40wt% coatings. The dashed line in black represents the control viral titer.

For HCoV, the inactivation kinetics data obtained over 24 hours at room-temperature showed the virus was unstable and self-inactivated in 24 hours (figure 4.17). While the stability of HCoV on surface for up to 6 days is reported in literature, the characteristics of the surface greatly influence virus persistence [44]. mbPP is hydrophobic with high filtration efficiency [62] and may accelerate virus inactivation or interfere with virus recovery. In 6 hours, the 30 and 40 wt% 6-OHDA based coatings showed 2.5 and 2.6-log reduction in the titer of HCoV respectively corresponding to > 99.9% reduction of the viral load (figure 4.17 A and B). This reduction in the titer of HCoV was significantly different than the control virus titer (per ANOVA analysis, p value = 0.03). The bare and control coated fabrics also showed 1.1 log-reduction in HCoV titer. In 24 hours, the titer of HCoV reduced to limit of detection values with both the control and catechol containing coatings. The reduction in virus titer may be due to the interaction between the fabric or incomplete recovery of virus solution from the fabric following incubation. A similar observation was made for HCoV with functionalized sbPP in section 4.2, where reduction in HCoV was observed despite a lack of virucidal activity. While the results indicate that HCoV can be self-inactivated, the coated fabrics were able to accelerate this inactivation process. Additionally, the active virucidal ingredient, H_2O_2 was cytotoxic to MRC5 cells, the indicator cell line utilized in assessing HCoV infectivity (figure 7.2 A and B). As a result, it is possible that the observed viral titers were actually higher than actual viral titers.
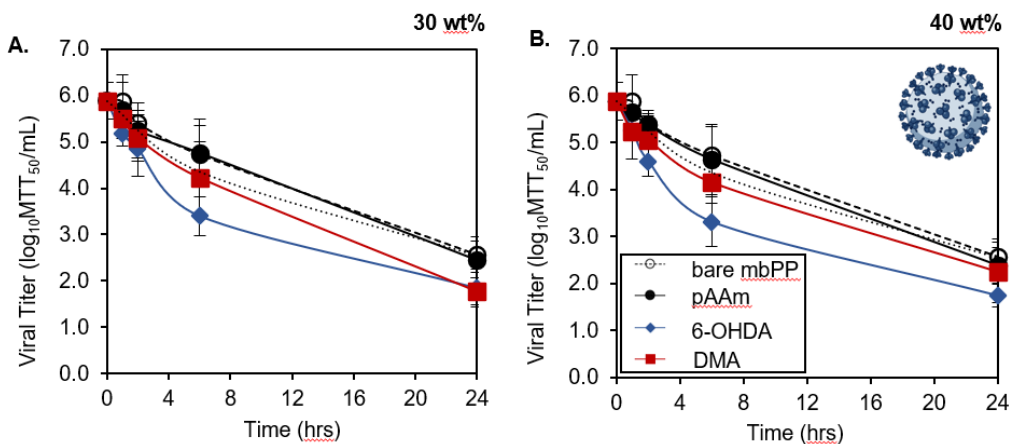
Figure 4.17: Time-dependent inactivation of HCoV. A drop of crude HCoV solution was incubated with bare and coated non-woven mbPP for 0,1, 2, 6 and 24 hours at room temperature to provide A. inactivation kinetics for 30wt% coatings and B. 40wt% coatings. The dashed line in black represents the control viral titer.

A first order model of inactivation described by equation 4.5 was fit to linearized inactivaion kinetics data obtained for both BVDV and HCoV (figure 4.18 and 4.19 respectively). The observed rate constant of inactivation (*k*) for the 6-OHDA and DMA

based copolymer coatings were estimated as previously described. For BVDV, kinetic data over 24 hours was used. The R^2 values observed (>0.75) showed the model fit the data relatively well. Novel 6-OHDA based coating was more effective than DMA as demonstarted by the considerably higher rate constants (figure 4.20A). There was no significant difference (p value > 0.05) between the 30 wt% and 40 wt% 6-OHDA coatings themselves. For HCoV, inactivation data upto 6 hours was used to obtain the first order model inactivation rate constant (figure 4.20B). Once again, the high R^2 (>0.75) values suggested realtively good fits of the model. For HCoV as well, the 6-OHDA based coatings showed significantly higher k values in comparison to the DMA based coatings. The obtained k value was also higher than that observed for the virus control (significant findign, p value < 0.05). The same data with a summary of the rate constants and the relative quantitation of the fit are tabulated in table 4.4.
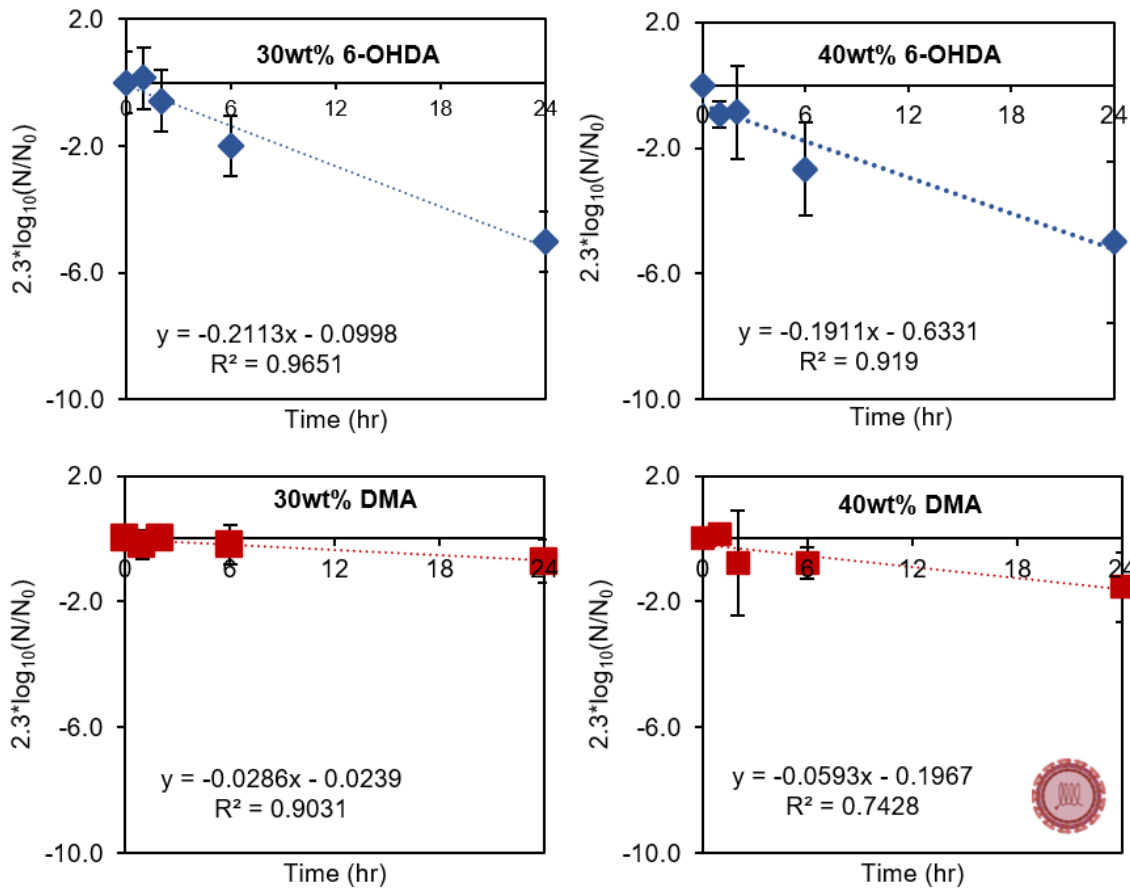
Figure 4.18: BVDV inactivation data for 0 ,1, 2, 6 and 24 hrs fit to a first order model of virus inactivation to obtain the constant rate of inactivation for the 30wt% and 40wt% 6-OHDA and DMA coated samples.
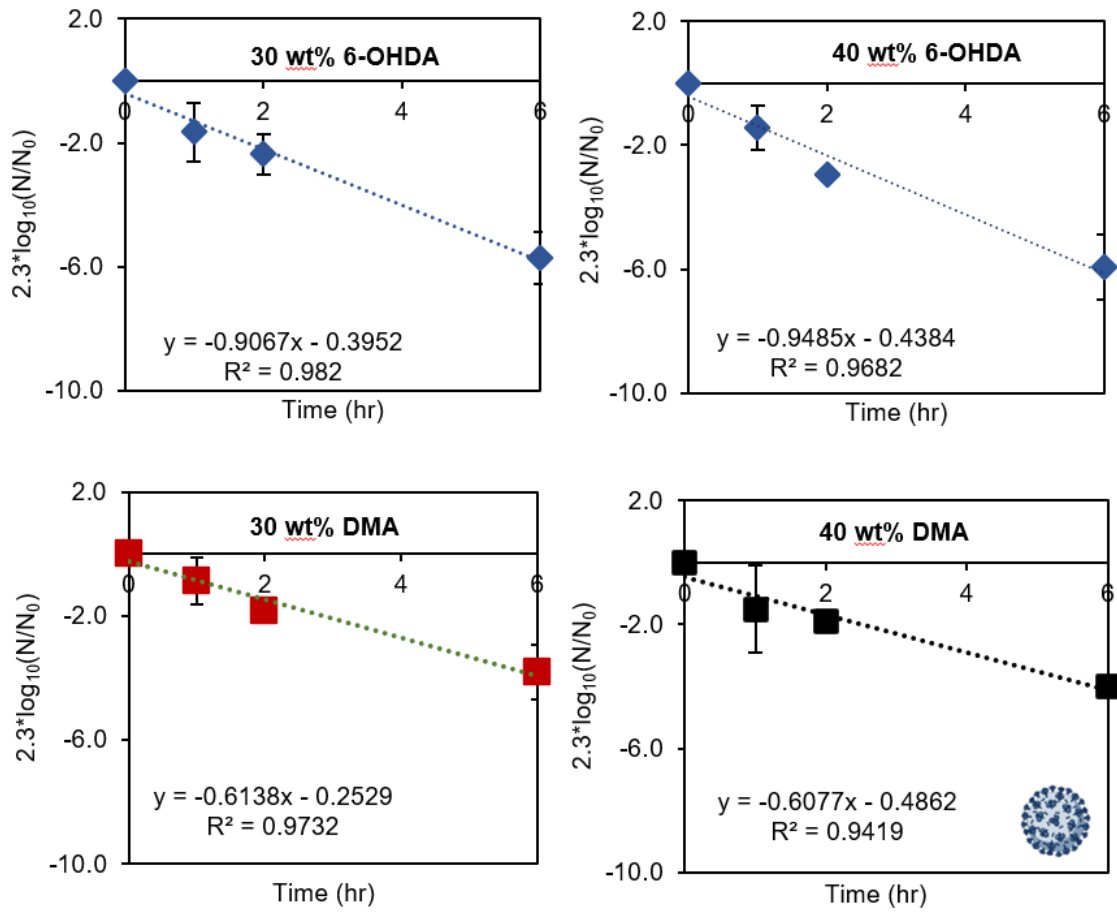
Figure 4.19: Linearized inactivation curves for first order inactivation kinetics agaisnt HCoV (left) with the observed inactivation rate constant (right) obtained as the slope of the linear model fit to the data for the catechol containing samples
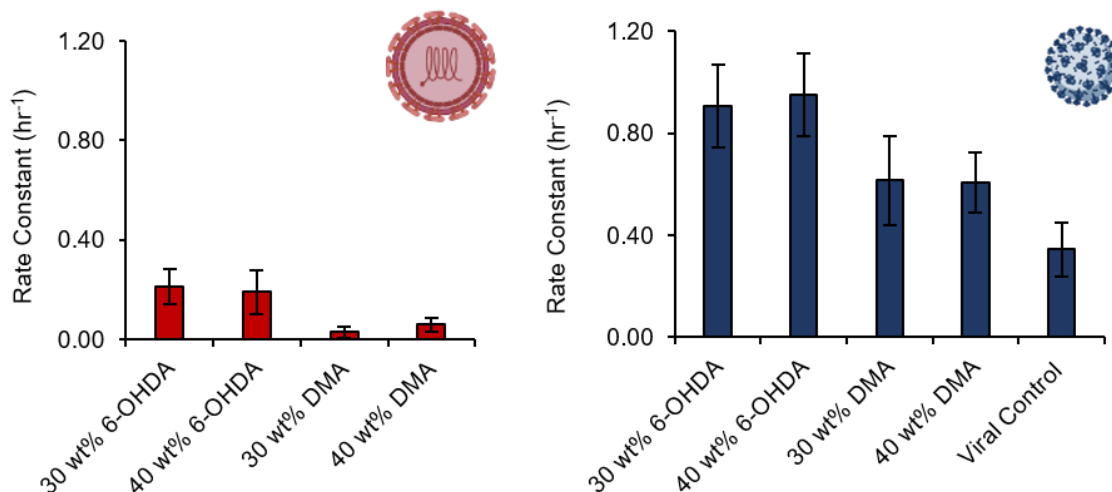
Figure 4.20: First order rate constants observed for HCoV (left in red) over 6 hours and BVDV (right in blue) over 24 hours; BVDV remained stable at room temperature over the 24-hour duration, therefore, self-inactivation rate constant for BVDV is not reported.

Table 4.4: Summary of observed inactivation rate constants obtained by fitting BVDV and HCoV time-dependent inactivation data to linearized 1st order model of virus inactivation.

Sample	Virus	Time (hrs)	1st order k (s^{-1})	1st order R^2
30 wt% DMA p			0.03	0.90
40 wt% DMA p			0.06	0.74
	BVDV	24		
30 wt% 6-OHDA p			0.21	0.97
40 wt% 6-OHDA p			0.19	0.92
30 wt% DMA p			0.61	0.97
40 wt% DMA p			0.61	0.94
	HCoV	6		
30 wt% 6-OHDA p			0.91	0.98
40 wt% 6-OHDA p			0.95	0.97

A novel antipathogenic copolymer coating, AA-DA-OH-co-AAM, was developed for non-woven mbPP fabrics, often utilized as the filtration layer of N95 masks.

Application of the coating did not impact fabric porosity considerably, a characteristic property crucial to maintaining filtration efficiency and breathability in masks. The coatings reduced the viral loads of both BVDV and HCoV by more than 99% in 24 hours and 6 hours respectively at room temperature. Varying the weight concentration of the catechol containing copolymer from 30 wt% to 40wt% did not significantly affect the performance of the coating against the model viruses. The fabrics, did however, show superior virucidal performance to an alternate catechol containing coating prepared by replacing 6-ODHA with DMA. The virucidal agent, H_2O_2 was released continuously in mM quantities in the presence of moisture at physiological pH 7.4. This concentration is much lower than those commonly used in hydrogen peroxide-based disinfection platforms. Moreover, H_2O_2 degrades into biocompatible products water and hydrogen, making it a suitable environmentally friendly alternative to harsh chemicals to reduce pathogenic load and mitigate disease transmission.

5 Conclusion

In summary, three novel virucidal materials namely, cupric-ion infused vermiculite and sepiolite, quaternary compound functionalized mbPP and sbPP fabrics and catechol copolymerized mbPP fabrics were developed. The virucidal activity of each of the materials were determined along with the mechanism which facilitated inactivation. An insight into the biological and physicochemical properties of virus and the main route of disease transmission were crucial to understanding the mechanism of inactivation of each of the novel materials.

Cupric-ion infused vermiculite and sepiolite required surface attachment of virus for inactivation. ICP-MS testing showed displacement of Mg^{2+} in the Cu^{2+} infused clay mineral samples. However, very low release of Cu^{2+} was observed in solution, suggesting majority of the antiviral ions remained within the clay mineral powder in suspension. This finding was supported by tests conducted with a metal-ion chelating and a blocking agent EDTA and BSA respectively. Virus size affected the extent of inactivation in the vermiculite powders. The smaller size of PPV relative to the pore size of vermiculite enabled better inactivation in comparison to the much larger HCoV. Sepiolite reduced virus burden by both, removal through adsorption, and inactivation with cupric-ions.

QA functionalized mbPP and sbPP filters also required surface attachment for significant inactivation of enveloped viruses. Due to the high hydrophobicity of the functionalized sbPP filter, the wetting procedure employed in the study was not adequate to promote interaction of the viruses with the QA compound. Moreover, zeta potential values obtained for the functionalized filters showed maximum reversal in the surface charge density of only the QA grafted mbPP fabric. The highest reduction in virus titer for both SuHV and HCoV were observed for the QA grafted mbPP filter. Some inactivation of HCoV was observed with the QA grafted and QA physisorbed sbPP filters. However, this reduction was comparable with the bare sbPP filter, suggesting either an inability to completely elute HCoV from the filter following incubation or self-inactivation of HCoV due to the interactions between the virus and surface of the filter.

Catechol copolymerized mbPP fabric utilized the moisture (H_2O) from the crude virus solution (in PBS) to oxidize the co-polymer catechol groups and generate the highly potent antiviral agent, H_2O_2. Relatively low concentrations, 1- 4 mM H_2O_2, were generated over 24 hours. These low concentrations were sufficient to show virucidal activity against the enveloped viruses BVDV and HCoV. Stability issues were observed with HCoV at room temperature over the testing period of 24 hours. The instability may be linked to virus-surface interactions (surface and virus hydrophobicity) and environmental factors such as temperature and humidity.

Each novel coating demonstrated substantial virucidal activity with excellent prospects to control direct and in-direct transmission of diseases. However, more research can be done to unleash the full potential of these novel virucidal materials. While the clay minerals reduced virus titer, little in known about the longevity of their antiviral property. Experiments can be conducted to explore (1) quantity of virus required to saturate the

coating and (2) duration over which the coating retains its antiviral property. Moreover, the studies conducted used a fixed concentration of copper containing clay mineral powder and a fixed temperature for virus treatment. Higher concentrations of the powder and incubation of virus at different temperatures may provide more insight towards the robustness of their application for high frequency touch surfaces. For the QA functionalized coatings, a C_{12} benzophenone compound was used. A grafting (covalent) application with the mbPP filter yielded promising results, however the same were not true for the sbPP filter. Further optimization by using a QA compatible more suitable for sbPP filters may extend the use of this application to surgical masks which often use sbPP as the outermost layer. Moreover, a single virus -filter incubation time point was explored in the study to demonstrate virucidal activity. A time-dependent kinetic model can be developed by exploring more contact times. Lastly, for the catechol copolymer coating on mbPP filters, a real-world application would require a virus aerosol to settle on the mask surface to activate the coating. The results presented in the study used a large droplet of crude virus solution which differs in properties from an aerosol (smaller hydrodynamic diameter). A system which contacts virus aerosols with the fabric is currently under work to mimic a more real-life scenario.

6 Reference List

1.   Services, D.o.H.a.H. *Severe Acute Respiratory Syndrome (SARS)*. 2004
        01/18/2023]; Available from: https://www.cdc.gov/sars/about/fs-SARS.pdf.
2.   Hasan, S., et al., *Ebola virus: A global public health menace: A narrative review.*
        J Family Med Prim Care, 2019. **8**(7): p. 2189-2201.
3.   Noorbakhsh, F., et al., *Zika Virus Infection, Basic and Clinical Aspects: A Review
        Article.* Iran J Public Health, 2019. **48**(1): p. 20-31.
4.   Prevention, C.f.D.C.a., *COVID Data Tracker.* 2022.
5.   Jayaweera, M., et al., *Transmission of COVID-19 virus by droplets and aerosols:
        A critical review on the unresolved dichotomy.* Environ Res, 2020. **188**: p.
        109819.
6.   van Seventer, J.M. and N.S. Hochberg, *Principles of Infectious Diseases:
        Transmission, Diagnosis, Prevention, and Control.*
7.   Kaushik, N., et al., *The inactivation and destruction of viruses by reactive oxygen
        species generated through physical and cold atmospheric plasma techniques:
        Current status and perspectives.* Journal of Advanced Research, 2023. **43**: p. 59-
        71.
8.   Sorlini, S., et al., *Appropriate technologies for drinking water treatment in
        Mediterranean countries.* Environmental Engineering and Management Journal,
        2015. **14**: p. 1721-1733.
9.   Bazant, M.Z. and J.W.M. Bush, *A guideline to limit indoor airborne transmission
        of COVID-19.* Proc Natl Acad Sci U S A, 2021. **118**(17).
10.   Zhang, N. and Y. Li, *Transmission of Influenza A in a Student Office Based on
        Realistic Person-to-Person Contact and Surface Touch Behaviour.* Int J Environ
        Res Public Health, 2018. **15**(8).
11.   Louten, J., *Virus Transmission and Epidemiology.* Essential Human Virology,
        2016: p. 71-92.
12.   Taylor, M.W., *What is a Virus? Viruses and Man: A History of Interactions.*
        2014(22): p. 23–40.
13.   Morawska, L. and G. Buonanno, *The physics of particle formation and deposition
        during breathing.* Nature Reviews Physics, 2021. **3**(5): p. 300-301.
14.   Louten, J., *Virus Structure and Classification*, in *Essential Human Virology.*
        2016. p. 19-29.
15.   Tournier, P., *[Definition, Structure and Classification of the Viruses].* Bull Mem
        Soc Med Hop Paris, 1964. **115**: p. 1259-64.
16.   Rakowska, P.D., et al., *Antiviral surfaces and coatings and their mechanisms of
        action.* Communications Materials, 2021. **2**(1): p. 53.
17.   Goodwin, C.M., S. Xu, and J. Munger, *Stealing the Keys to the Kitchen: Viral
        Manipulation of the Host Cell Metabolic Network.* Trends Microbiol, 2015.
        23(12): p. 789-798.
18.   J, L., - *Virus Replication.* Essential Human Virology, 2016: p. 00004-1.
19.   Mettlen, M., et al., *Regulation of Clathrin-Mediated Endocytosis.* Annu Rev
        Biochem, 2018. **87**: p. 871-896.

20.   Kiss, A.L. and E. Botos, *Endocytosis via caveolae: alternative pathway with distinct cellular compartments to avoid lysosomal degradation?* J Cell Mol Med, 2009. **13**(7): p. 1228-37.

21.   Dimitrov, D.S., *VIRUS ENTRY: MOLECULAR MECHANISMS AND BIOMEDICAL APPLICATIONS.* Nature Reviews, 2004(2): p. 109-122.

22.   Rey, F.A. and S.M. Lok, *Common Features of Enveloped Viruses and Implications for Immunogen Design for Next-Generation Vaccines.* Cell, 2018. **172**(6): p. 1319-1334.

23.   Mateu, M.G., *Structure and physics of viruses.* Thematic issue of Subcell, 2013: p. 12.

24.   de Pablo, P.J. and M.G. Mateu, *Mechanical Properties of Viruses*, in *Structure and Physics of Viruses: An Integrated Textbook*, M.G. Mateu, Editor. 2013, Springer Netherlands: Dordrecht. p. 519-551.

25.   Chaitanya, K.V., *Structure and Organization of Virus Genomes*, in *Genome and Genomics: From Archaea to Eukaryotes*, K.V. Chaitanya, Editor. 2019, Springer Singapore: Singapore. p. 1-30.

26.   J, L., - *Viral Membranes.* Encyclopedia of Virology, 2008: p. 00530-6.

27.   Su, X., et al., *Protein- and Peptide-Based Virus Inactivators: Inactivating Viruses Before Their Entry Into Cells.* Frontiers in Microbiology, 2020. **11**.

28.   Ge, Y., et al., *Kinetics and Mechanisms of Virus Inactivation by Chlorine Dioxide in Water Treatment: A Review.* Bull Environ Contam Toxicol, 2021. **106**(4): p. 560-567.

29.   Wisskirchen, K., et al., *New pharmacological strategies to fight enveloped viruses.* Trends in Pharmacological Sciences, 2014. **35**(9): p. 470-478.

30.   Firquet, S., et al., *Survival of Enveloped and Non-Enveloped Viruses on Inanimate Surfaces.* Microbes Environ, 2015. **30**(2): p. 140-4.

31.   Macinga, D.R., et al., *Improved Inactivation of Nonenveloped Enteric Viruses and Their Surrogates by a Novel Alcohol-Based Hand Sanitizer.* Applied and Environmental Microbiology, 2008. **74**(16): p. 5047-5052.

32.   Kampf, G., et al., *Persistence of coronaviruses on inanimate surfaces and their inactivation with biocidal agents.* Journal of Hospital Infection, 2020. **104**(3): p. 246-251.

33.   Ausar, S.F., et al., *Conformational Stability and Disassembly of Norwalk Virus-like Particles: EFFECT OF pH AND TEMPERATURE*.* Journal of Biological Chemistry, 2006. **281**(28): p. 19478-19488.

34.   Boschetti, N., et al., *Stability of minute virus of mice against temperature and sodium hydroxide.* Biologicals, 2003. **31**(3): p. 181-185.

35.   Oliveira, A.C., et al., *Low Temperature and Pressure Stability of Picornaviruses: Implications for Virus Uncoating.* Biophysical Journal, 1999. **76**(3): p. 1270-1279.

36.   Hogle, J., M. Chow, and D. Filman, *Three-dimensional structure of poliovirus at 2.9 Å resolution.* Science, 1985. **229**(4720): p. 1358-1365.

37.   Rossmann, M.G., et al., *Structure of a human common cold virus and functional relationship to other picornaviruses.* Nature, 1985. **317**(6033): p. 145-153.

38. Acharya, R., et al., *The three-dimensional structure of foot-and-mouth disease virus at 2.9 Å resolution.* Nature, 1989. **337**(6209): p. 709-716.

39. Aganovic, A., et al., *Modeling the impact of indoor relative humidity on the infection risk of five respiratory airborne viruses.* Sci Rep, 2022. **12**(1): p. 11481.

40. Mocé-Llivina, L., G.T. Papageorgiou, and J. Jofre, *A membrane-based quantitative carrier test to assess the virucidal activity of disinfectants and persistence of viruses on porous fomites.* Journal of Virological Methods, 2006. **135**(1): p. 49-55.

41. Yang, W. and L.C. Marr, *Mechanisms by which ambient humidity may affect viruses in aerosols.* Appl Environ Microbiol, 2012. **78**(19): p. 6781-8.

42. Owen, L., et al., *Porous surfaces: stability and recovery of coronaviruses.* Interface Focus, 2022. **12**(1): p. 20210039.

43. Fuhs, G.W., et al., *Virus adsorption to mineral surfaces is reduced by microbial overgrowth and organic coatings.* Microb Ecol, 1985. **11**(1): p. 25-39.

44. Wang, X. and V.V. Tarabara, *Virus adhesion to archetypal fomites: A study with human adenovirus and human respiratory syncytial virus.* Chemical Engineering Journal, 2022. **429**: p. 132085.

45. Chin, A.W.H., et al., *Stability of SARS-CoV-2 in different environmental conditions.* Lancet Microbe, 2020. **1**(1): p. e10.

46. Chattopadhyay, D., et al., *Effect of Surfactants on the Survival and Sorption of Viruses.* Environmental Science & Technology, 2002. **36**(19): p. 4017-4024.

47. Bhardwaj, R. and A. Agrawal, *How coronavirus survives for days on surfaces.* Phys Fluids (1994), 2020. **32**(11): p. 111706.

48. Collins, A.P., et al., *N95 respirator and surgical mask effectiveness against respiratory viral illnesses in the healthcare setting: A systematic review and meta-analysis.* J Am Coll Emerg Physicians Open, 2021. **2**(5): p. e12582.

49. Dugdale, C.M. and R.P. Walensky, *Filtration Efficiency, Effectiveness, and Availability of N95 Face Masks for COVID-19 Prevention.* JAMA Internal Medicine, 2020. **180**(12): p. 1612-1613.

50. Verbeek, J.H., et al., *Personal protective equipment for preventing highly infectious diseases due to exposure to contaminated body fluids in healthcare staff.* Cochrane Database Syst Rev, 2020. **4**(4): p. Cd011621.

51. Chan, Y.F. and S. Abu Bakar, *Virucidal activity of Virkon S on human enterovirus.* Med J Malaysia, 2005. **60**(2): p. 246-8.

52. Gerba, C.P., *Quaternary ammonium biocides: efficacy in application.* Appl Environ Microbiol, 2015. **81**(2): p. 464-9.

53. Juszkiewicz, M., M. Walczak, and G. Woźniakowski, *Characteristics of Selected Active Substances used in Disinfectants and their Virucidal Activity Against ASFV.* J Vet Res, 2019. **63**(1): p. 17-25.

54. Lin, Q., et al., *Sanitizing agents for virus inactivation and disinfection.* VIEW, 2020. **1**(2): p. e16.

55. McDonnell, G. and A.D. Russell, *Antiseptics and disinfectants: activity, action, and resistance.* Clin Microbiol Rev, 1999. **12**(1): p. 147-79.

56. Wessels, S. and H. Ingmer, *Modes of action of three disinfectant active substances: A review.* Regulatory Toxicology and Pharmacology, 2013. **67**(3): p. 456-467.

57. Wigginton, K.R., et al., *Virus Inactivation Mechanisms: Impact of Disinfectants on Virus Function and Structural Integrity.* Environmental Science & Technology, 2012. **46**(21): p. 12069-12078.

58. Farzaneh, S. and M. Shirinbayan, *Processing and Quality Control of Masks: A Review.* Polymers (Basel), 2022. **14**(2).

59. Kara, Y. and K. Molnár, *A review of processing strategies to generate melt-blown nano/microfiber mats for high-efficiency filtration applications.* Journal of Industrial Textiles, 2021. **51**(1_suppl): p. 137S-180S.

60. Spennemann, D.H.R., *Environmental Decay of Single Use Surgical Face Masks as an Agent of Plastic Micro-Fiber Pollution.* Environments, 2022. **9**(7): p. 94.

61. Das, S., et al., *A comprehensive review of various categories of face masks resistant to Covid-19.* Clinical Epidemiology and Global Health, 2021. **12**: p. 100835.

62. Tsutsumi-Arai, C., et al., *Surface Functionalization of Non-Woven Fabrics Using a Novel Silica-Resin Coating Technology: Antiviral Treatment of Non-Woven Fabric Filters in Surgical Masks.* Int J Environ Res Public Health, 2022. **19**(6).

63. Patterson, E.I., et al., *Methods of Inactivation of SARS-CoV-2 for Downstream Biological Assays.* The Journal of Infectious Diseases, 2020. **222**(9): p. 1462-1467.

64. Wang, J., et al., *Virus inactivation and protein recovery in a novel ultraviolet-C reactor.* Vox Sang, 2004. **86**(4): p. 230-8.

65. Eterpi, M., G. McDonnell, and V. Thomas, *Disinfection efficacy against parvoviruses compared with reference viruses.* J Hosp Infect, 2009. **73**(1): p. 64-70.

66. Jeong, E.K., J.E. Bae, and I.S. Kim, *Inactivation of influenza A virus H1N1 by disinfection process.* Am J Infect Control, 2010. **38**(5): p. 354-60.

67. Abu-Aisha, H., et al., *The effect of chemical and heat disinfection of the hemodialysis machines on the spread of hepatitis C virus infection: a prospective study.* Saudi J Kidney Dis Transpl, 1995. **6**(2): p. 174-8.

68. Gamble, A., et al., *Heat-Treated Virus Inactivation Rate Depends Strongly on Treatment Procedure: Illustration with SARS-CoV-2.* Applied and Environmental Microbiology, 2021. **87**(19): p. e00314-21.

69. Sadraeian, M., et al., *Viral inactivation by light.* eLight, 2022. **2**(1): p. 18.

70. Dhama, K., et al., *The role of disinfectants and sanitizers during COVID-19 pandemic: advantages and deleterious effects on humans and the environment.* Environ Sci Pollut Res Int, 2021. **28**(26): p. 34211-34228.

71. Sagripanti, J.L., L.B. Routson, and C.D. Lytle, *Virus inactivation by copper or iron ions alone and in the presence of peroxide.* Appl Environ Microbiol, 1993. **59**(12): p. 4374-6.

72. Maillard, J.-Y., et al., *Efficacy and mechanisms of action of sodium hypochlorite on Pseudomonas aeruginosa PAO1 phage F116.* Journal of Applied Microbiology, 1998. **85**(6): p. 925-932.

73. Ishihara, M., et al., *Stability of Weakly Acidic Hypochlorous Acid Solution with Microbicidal Activity.* Biocontrol Science, 2017. **22**(4): p. 223-227.

74. Vereshchagin, A.N., et al., *Quaternary Ammonium Compounds (QACs) and Ionic Liquids (ILs) as Biocides: From Simple Antiseptics to Tunable Antimicrobials.* International Journal of Molecular Sciences, 2021. **22**(13): p. 6793.

75. Caschera, A.G., et al., *Evaluation of virucidal activity of residual quaternary ammonium-treated surfaces on SARS-CoV-2.* Am J Infect Control, 2022. **50**(3): p. 325-329.

76. Baker, N., et al., *Repurposing Quaternary Ammonium Compounds as Potential Treatments for COVID-19.* Pharm Res, 2020. **37**(6): p. 104.

77. Omidbakhsh, N. and S.A. Sattar, *Broad-spectrum microbicidal activity, toxicologic assessment, and materials compatibility of a new generation of accelerated hydrogen peroxide-based environmental surface disinfectant.* American Journal of Infection Control, 2006. **34**(5): p. 251-257.

78. Davies, R.L. and S.F. Etris, *The development and functions of silver in water purification and disease control.* Catalysis Today, 1997. **36**(1): p. 107-114.

79. Bright, K.R., et al., *Assessment of the Antiviral Properties of Zeolites Containing Metal Ions.* Food and Environmental Virology, 2009. **1**(1): p. 37-41.

80. Warnes, S.L., Z.R. Little, and C.W. Keevil, *Human Coronavirus 229E Remains Infectious on Common Touch Surface Materials.* mBio, 2015. **6**(6): p. e01697-15.

81. Govind, V., et al., *Antiviral properties of copper and its alloys to inactivate covid-19 virus: a review.* Biometals, 2021. **34**(6): p. 1217-1235.

82. Manoharan, K. and S. Bhattacharya, *Superhydrophobic surfaces review: Functional application, fabrication techniques and limitations.* Journal of Micromanufacturing, 2019. **2**(1): p. 59-78.

83. Wang, S., L. Feng, and L. Jiang, *One-Step Solution-Immersion Process for the Fabrication of Stable Bionic Superhydrophobic Surfaces.* Advanced Materials, 2006. **18**(6): p. 767-770.

84. Falde, E.J., et al., *Superhydrophobic materials for biomedical applications.* Biomaterials, 2016. **104**: p. 87-103.

85. Zhong, H., et al., *Reusable and Recyclable Graphene Masks with Outstanding Superhydrophobic and Photothermal Performances.* ACS Nano, 2020. **14**(5): p. 6213-6221.

86. Zhu, P., et al., *Superhydrophobicity preventing surface contamination as a novel strategy against COVID-19.* J Colloid Interface Sci, 2021. **600**: p. 613-619.

87. Galdiero, S., et al., *Silver Nanoparticles as Potential Antiviral Agents.* Molecules, 2011. **16**(10): p. 8894-8918.

88. Arvizo, R.R., et al., *Intrinsic therapeutic applications of noble metal nanoparticles: past, present and future.* Chemical Society Reviews, 2012. **41**(7): p. 2943-2970.

89. Maduray, K. and R. Parboosing, *Metal Nanoparticles: a Promising Treatment for Viral and Arboviral Infections.* Biol Trace Elem Res, 2021. **199**(8): p. 3159-3176.

90. Jeremiah, S.S., et al., *Potent antiviral effect of silver nanoparticles on SARS-CoV-2.* Biochem Biophys Res Commun, 2020. **533**(1): p. 195-200.

91. Xiang, D.X., et al., *Inhibitory effects of silver nanoparticles on H1N1 influenza A virus in vitro.* J Virol Methods, 2011. **178**(1-2): p. 137-42.

92. Lara, H.H., et al., *Mode of antiviral action of silver nanoparticles against HIV-1.* J Nanobiotechnology, 2010. **8**: p. 1.

93. Toledo, E., et al., *Nanocomposite coatings for the prevention of surface contamination by coronavirus.* PLoS One, 2022. **17**(8): p. e0272307.

94. Alavi, M., et al., *Metal and metal oxide-based antiviral nanoparticles: Properties, mechanisms of action, and applications.* Advances in Colloid and Interface Science, 2022. **306**: p. 102726.

95. Hamdi, M., et al., *Investigating the Internalization and COVID-19 Antiviral Computational Analysis of Optimized Nanoscale Zinc Oxide.* ACS Omega, 2021. **6**(10): p. 6848-6860.

96. Kumar, R., et al., *Iron oxide nanoparticles based antiviral activity of H1N1 influenza A virus.* Journal of Infection and Chemotherapy, 2019. **25**(5): p. 325-329.

97. Syngouna, V.I. and C.V. Chrysikopoulos, *Interaction between Viruses and Clays in Static and Dynamic Batch Systems.* Environmental Science & Technology, 2010. **44**(12): p. 4539-4544.

98. Rius-Rocabert, S., et al., *Broad virus inactivation using inorganic micro/nano-particulate materials.* Mater Today Bio, 2022. **13**: p. 100191.

99. Das, P. and B.V. Tadikonda, *Bentonite Clay: A Potential Natural Sanitizer for Preventing Neurological Disorders.* ACS Chem Neurosci, 2020. **11**(20): p. 3188-3190.

100. Heldt, C.L., et al., *A colorimetric assay for viral agents that produce cytopathic effects.* Journal of Virological Methods, 2006. **135**(1): p. 56-65.

101. Sharma, V., *Cupric ion infused vermiculite and sepiolite require surface adsorption for virus inactivation.* In prep.

102. Sorci, M., et al., *Virucidal N95 Respirator Face Masks via Ultrathin Surface-Grafted Quaternary Ammonium Polymer Coatings.* ACS Appl Mater Interfaces, 2022. **14**(22): p. 25135-25146.

103. Raghavan, P., et al., *Ionic conductivity and electrochemical properties of nanocomposite polymer electrolytes based on electrospun poly(vinylidene fluoride-co-hexafluoropropylene) with nano-sized ceramic fillers.* Electrochimica Acta, 2008. **54**(2): p. 228-234.

104. Clement, M.-V., et al., *The cytotoxicity of dopamine may be an artefact of cell culture.* Journal of neurochemistry, 2002. **81**: p. 414-21.

105. Arendsen, L.P., R. Thakar, and A.H. Sultan, *The Use of Copper as an Antimicrobial Agent in Health Care, Including Obstetrics and Gynecology.* Clin Microbiol Rev, 2019. **32**(4).

106. Mertens, B.S., et al., *Efficacy and Mechanisms of Copper Ion-Catalyzed Inactivation of Human Norovirus.* ACS Infectious Diseases, 2022. **8**(4): p. 855-864.

107. Qian, Y., et al., *Synthesis and Properties of Vermiculite-Reinforced Polyurethane Nanocomposites.* ACS Applied Materials & Interfaces, 2011. **3**(9): p. 3709-3717.

108.   Williams, L., et al., *Killer Clays! Natural antibacterial clay minerals.* Mineralogical Society Bulletin, 2004. **139**.

109.   García-Villén, F. and C. Viseras, *Clay-Based Pharmaceutical Formulations and Drug Delivery Systems.* Pharmaceutics, 2020. **12**(12).

110.   Low, N.M.P., *The Thermal Insulating Properties of Vermiculite.* Journal of Thermal Insulation, 1984. **8**(2): p. 107-115.

111.   Alvarez, A., *Sepiolite: Properties and Uses*, in *Developments in Sedimentology*, A. Singer and E. Galan, Editors. 1984, Elsevier. p. 253-287.

112.   Drelich, J., *Vermiculite decorated with copper nanoparticles: Novel antibacterial hybrid material.* Applied Surface Science, 2011: p. 9435-9443.

113.   Jampa, S., et al., *Transparent Anti-SARS COV-2 Film from Copper(I) Oxide Incorporated in Zeolite Nanoparticles.* ACS Applied Materials & Interfaces, 2022. **14**(46): p. 52334-52346.

114.   Sifang Steve, Z., *Variability and Relative Order of Susceptibility of Non-Enveloped Viruses to Chemical Inactivation*, in *Disinfection of Viruses*, W.N. Raymond and M.K. Ijaz, Editors. 2022, IntechOpen: Rijeka. p. Ch. 6.

115.   Hiatt, C.W., *Kinetics of the Inactivation of Viruses.* Bacteriol Rev, 1964. **28**(2): p. 150-63.

116.   Janica, I., et al., *Thermal insulation with 2D materials: liquid phase exfoliated vermiculite functional nanosheets.* Nanoscale, 2018. **10**(48): p. 23182-23190.

117.   Li, H., et al., *Efficacy and practice of facemask use in general population: a systematic review and meta-analysis.* Translational Psychiatry, 2022. **12**(1): p. 49.

118.   Brooks, J.T. and J.C. Butler, *Effectiveness of Mask Wearing to Control Community Spread of SARS-CoV-2.* JAMA, 2021. **325**(10): p. 998-999.

119.   Rogak, S.N., et al., *Properties of materials considered for improvised masks.* Aerosol Science and Technology, 2021. **55**(4): p. 398-413.

120.   Allison, B.C., B.M. Applegate, and J.P. Youngblood, *Hemocompatibility of Hydrophilic Antimicrobial Copolymers of Alkylated 4-Vinylpyridine.* Biomacromolecules, 2007. **8**(10): p. 2995-2999.

121.   Gao, J., et al., *Surface Grafted Antimicrobial Polymer Networks with High Abrasion Resistance.* ACS Biomaterials Science & Engineering, 2016. **2**(7): p. 1169-1179.

122.   Benskey, M.J. and F.P. Manfredsson, *Lentivirus Production and Purification.* Methods Mol Biol, 2016. **1382**: p. 107-14.

123.   Kaur, S., et al., *Direct Observation of the Interplay of Catechol Binding and Polymer Hydrophobicity in a Mussel-Inspired Elastomeric Adhesive.* ACS Cent Sci, 2018. **4**(10): p. 1420-1429.

124.   Amanna, I.J., H.-P. Raué, and M.K. Slifka, *Development of a new hydrogen peroxide–based vaccine platform.* Nature Medicine, 2012. **18**(6): p. 974-979.

125.   Meng, H., et al., *Biomimetic recyclable microgels for on-demand generation of hydrogen peroxide and antipathogenic application.* Acta Biomaterialia, 2019. **83**: p. 109-118.

126.   Dembinski, J.L., et al., *Hydrogen peroxide inactivation of influenza virus preserves antigenic structure and immunogenicity.* J Virol Methods, 2014. **207**: p. 232-7.

127. Hodgkinson, Victoria, and Michael J Petris. "Copper homeostasis at the host-pathogen interface." *The Journal of biological chemistry* vol. 287,17 (2012): 13549-55. doi:10.1074/jbc.R111.316406

128. Horie, M et al. "Inactivation and morphological changes of avian influenza virus by copper ions." *Archives of virology* vol. 153,8 (2008): 1467-72. doi:10.1007/s00705-008-0154-2

129. Minoshima, M. *et al.* (2016) "Comparison of the antiviral effect of solid-state copper and silver compounds," *Journal of Hazardous Materials*, 312, pp. 1–7. Available at: https://doi.org/10.1016/j.jhazmat.2016.03.023.

130. Nowak, T. V., Popp, B., & Roth, N. (2019). Choice of parvovirus model for validation studies influences the interpretation of the effectiveness of a virus filtration step. *Biologicals*, *60*, 85-92. https://doi.org/10.1016/j.biologicals.2019.04.003

131. Morris, Dylan H et al. "Mechanistic theory predicts the effects of temperature and humidity on inactivation of SARS-CoV-2 and other enveloped viruses." *eLife* vol. 10 e65902. 13 Jul. 2021, doi:10.7554/eLife.65902

7 Supplementary Data

7.1 Cupric-ion infused clay minerals

7.1.1 . ICP testing

Table 7.1: ICP testing of copper treated clay mineral powder with PBS for 2 hours (Provided by Dr. Bowen Li) with the amount of metal ion leached reported in parts per million (ppm)

Sample	Ca (ppm)	Cu (ppm)	Mg (ppm)	P (ppm)	Al (ppm)	Fe(ppm)
UnV-Cu	<0.05	<0.05	<0.05	110.5	<0.05	<0.05
V-Cu	64.81	0.087	52.58	134.2	<0.05	0.077
V	4.516	<0.05	41.46	75.93	<0.05	<0.05
S-Cu	195.5	<0.05	34.03	39.75	<0.05	<0.05
S	34.78	<0.05	17.51	114.5	<0.05	<0.05
Cu_2O	48.47	<0.05	64.74	95.54	<0.05	<0.05

Table 7.2: ICP testing of copper treated clay mineral powder with distilled water for 2 hours (Provided by Dr. Bowen Li) with the amount of metal ion leached reported in parts per million (ppm)

Sample	Ca (ppm)	Cu (ppm)	Mg (ppm)	P (ppm)	Al (ppm)	Fe(ppm)
UnV-Cu	0.298	0.325	<0.05	<0.05	<0.05	<0.05
V-Cu	174.1	<0.05	55.28	0.426	<0.05	<0.05
V	21.0	<0.05	8.3	0.1	<0.05	<0.05
S-Cu	438.7	<0.05	27.89	<0.05	<0.05	<0.05
S	-	-	-	-	-	-
Cu_2O	42.41	0.089	41.47	0.123	<0.05	0.164

7.2 C$_{12}$ quaternized non-woven filtration fabrics

7.2.1 FE and PE data obtained for full N95-mask and single ply mbPP filter
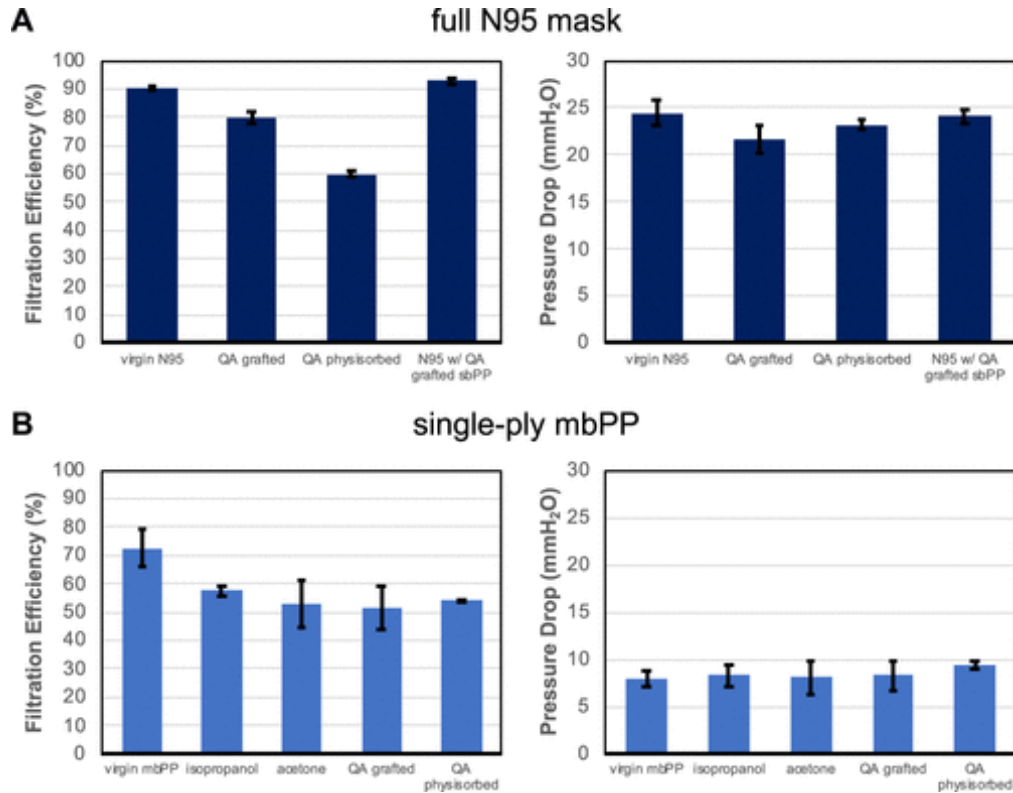

Figure 7.1: Comparing filtration efficiency for standard and modified N95 masks (A) and single ply mbPP (B). Figure reprinted from publication cited as reference # 102, Copyright 2022, Sorci et. al., published under license CC BY-NC-ND 4.0.

The filtration efficiency was determined using the NIOSH standard protocol used for certifying N95 respirator masks with slight modifications [102]. Aerosols of NaCl of the specified size distribution were tested at 9.4 cm/s face velocity. Particle counting and detection was accomplished using a condensation counter and differential mobility analyzer. Figure 7.1 shows results for both a full N95 masks, bare and coated (figure 7.1A) as well as a single ply melt-blown PP mask, bare and coated (Figure 7.1B).

7.3 Catechol copolymerized non-woven filter

7.3.1 Cytotoxicity of catechol coated filters
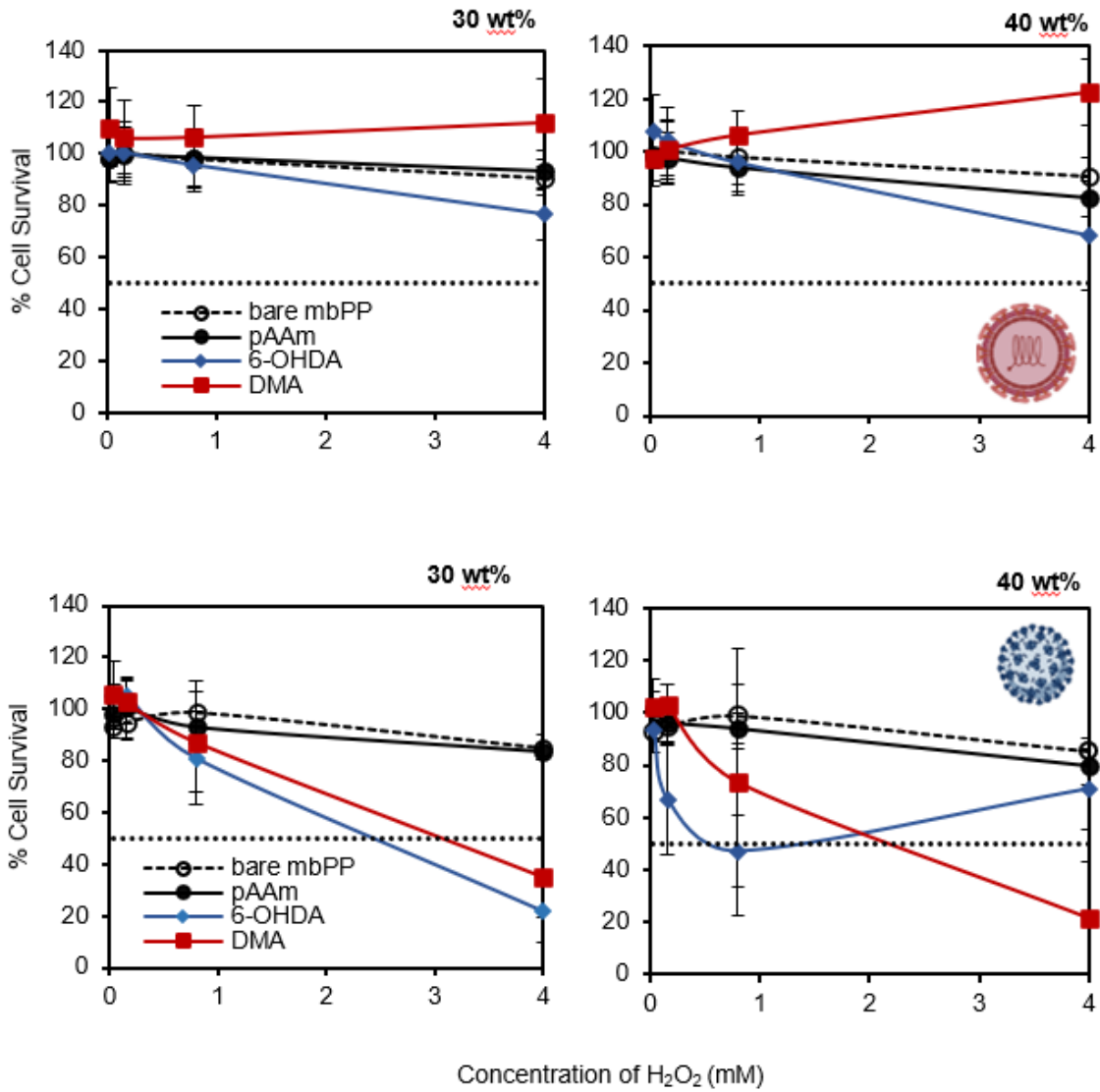
Figure 7.2: Cytotoxicity data for varying concentration of hydrogen peroxide against the indicator cell line A. BT cells for BVDV and B. MRC-5 cells for HCoV

8 Copyright documentation

Some of the images and data represented in this document were taken from a paper published in the ACS Applied Materials and Interfaces, which is a public domain, or licensed for reuse under a Creative Commons license - Attribution-NonCommercial-NoDerivatives 4.0 International (CC BY-NC-ND 4.0). Other images were created in biorender.com and cited as described by the platform. Please see below for full citation and attribution information.

Figures 3.1, 3.2, 4.10, 4.11 and 7.1 Source:

Sorci, M., et al., *Virucidal N95 Respirator Face Masks via Ultrathin Surface-Grafted Quaternary Ammonium Polymer Coatings.* ACS Appl Mater Interfaces, 2022. **14**(22): p. 25135-25146.

The figures were adapted from the above citation referenced as #102 in the document, Copyright 2022, Sorci et.al., under a CC BY-NC-ND 4.0 license.